Title
Sparse genetically-defined neurons refine canonical periaqueductal gray columnar organization

Author
La-Vu, My Quynh

Publication Date
2022

Peer reviewed|Thesis/dissertation

UNIVERSITY OF CALIFORNIA

Los Angeles

Sparse genetically-defined neurons refine canonical periaqueductal gray columnar organization

A dissertation submitted in partial satisfaction of the requirements for the degree

Doctor of Philosophy in Neuroscience

by

My Quynh La-Vu

2022

ABSTRACT OF THE DISSERTATION

Sparse genetically-defined neurons refine canonical periaqueductal gray columnar organization

by

My Quynh La-Vu

Doctor of Philosophy in Neuroscience

University of California, Los Angeles, 2022

Professor Avishek Adhikari, Chair

When encountering external threats, survival depends on the engagement of appropriate defensive reactions to minimize harm. There are major clinical implications for identifying the neural circuitry and activation patterns that produce such defensive reactions, as maladaptive overactivation of these circuits underlies pathological human anxiety and fear responses. A compelling body of work has linked activation of large glutamatergic neuronal populations in the midbrain periaqueductal gray (PAG) to defensive reactions such as freezing, flight and threat-induced analgesia. These pioneering data have firmly established that the overarching functional organization axis of the PAG is along anatomically-defined columnar boundaries. Accordingly, broad activation of the dorsolateral column induces flight, while activation of the lateral or ventrolateral (l and vl) columns induces freezing. However, the PAG contains a diverse arrangement of cell types that vary in neurochemical profile and location. How these cell types contribute to defensive responses remains largely unknown, indicating that targeting sparse, genetically-defined populations can lead to a deeper understanding of how the PAG generates a wide array of behaviors. Though several prior works showed that broad excitation of the lPAG or

vlPAG causes freezing, we found in mice that activation of lateral and ventrolateral PAG (l/vlPAG) cholecystokinin-expressing (cck) cells selectively caused flight to safer regions within an environment. Furthermore, inhibition of l/vlPAG-cck cells reduced avoidance of a predatory threat without altering other defensive behaviors like freezing. Lastly, l/vlPAG-cck activity decreased when approaching threat and increased during movement to safer locations. Taken together, these data suggest cck cells are driving threat avoidance states, which are epochs during which mice increase distance to the threat and perform evasive escape. In contrast, activating l/vlPAG cells pan-neuronally promoted freezing and these cells were activated near threat. These data underscore the importance of investigating genetically-identified PAG cells. Using this approach, we found a sparse population of cck-expressing l/vlPAG cells that have distinct and opposing function and neural activation motifs compared to the broader local ensemble defined solely by columnar anatomical boundaries. Thus, in addition to the anatomical columnar architecture of the PAG, the molecular identity of PAG cells may confer an additional axis of functional organization, revealing unexplored functional heterogeneity.

The dissertation of My Quynh La-Vu is approved.

Stephanie Correa

Michael S. Fanselow

Kate Wassum

Avishek Adhikari, Committee Chair

University of California, Los Angeles

2022

DEDICATION

To Mom, Dad, Cindy, and Alex –

Science gives the world definitions,

Love gives life meaning.

Thank you for your Love.

TABLE OF CONTENTS

LIST OF FIGURES

ACKNOWLEDGEMENTS

Science is a lot more fun when it is shared. I'd like to thank all the members of the Adhikari lab as well as the Cahill, Wassum, Correa, and Silva labs.

In particular, I'd like to thank Ekayana Sethi, who has been an honor to work with. I thank her for believing in me and entrusting her time and training with me. I look forward to all the incredible and awesome feats she will accomplish.

I thank Sandra Maesta-Pereira, who performed many of the early analyses of this project, and helped me develop my hypotheses and understand how to best test them. For this, I owe her a great deal of credit and gratitude.

I thank Dr. Peter Schuette for beginning his Ph.D. journey in parallel with mine. It has been amazing watching him work and he constantly inspires me to be as unequivocally brilliant and kind.

I thank Brooke Tobias (soon-to-be Dr. Tobias) for being the partner, friend, and confidante I needed at every stage of my doctoral work. She made my experience these past 4 years particularly lovely and colorful.

I thank Dr. Fernando Reis for his wholehearted dedication to the most rigorous research and careful science; it has been a constant source of inspiration. Most importantly, I thank him for the great friendship and deep kinship.

I thank Dr. Avishek Adhikari, whose mentorship has been an awesomely shaping and impactful experience. It has been a true honor to be trained by one of the most discerning scientific minds the world has to offer. It is even more heartening to have the belief and trust of someone as astute as he is. If I were to sum up his approach to science, it is, "Get things done, and have some fun." I hope he never stops!

To Dr. Denise Cai – From bean… to stalk!

I thank my committee members who have followed and guided my thesis for the past 4 years. I also thank Jenny Lee, Katherine Fang, and Dr. Felix Schweizer for their constant care and support.

To all, thank you for making science fun. Thank you for celebrating and commiserating. Keep finding out more about the world. Thank you for teaching me along the way.

VITA

2011 - 2015 B.A. in Psychology, University of California, Los Angeles, Los Angeles, CA

2017 - 2022 Ph.D. in Neuroscience, University of California, Los Angeles, Los Angeles, CA

PUBLICATIONS

La-Vu, M., Sethi, E., Maesta-Pereira, S., Schuette, P., Tobias, B., Reis, F., Wang, W., Torossian, A., Bishop, A., Leonard, S., Lin, L., Cahill, C., Adhikari, A. Sparse genetically-defined neurons refine the canonical role of periaqueductal gray columnar organization. *eLife* (2022). doi.org/10.7554/eLife.77115

La-Vu, M.*, Tobias, B. C.*, Schuette, P. J., Adhikari, A. To Approach or Avoid: An Introductory Overview of the Study of Anxiety Using Rodent Assays. *Frontiers in behavioral neuroscience* **14**, (2020). doi.org/10.3389/fnbeh.2020.00145

Wang, W., Schuette, P. J., **La-Vu, M.**, Torrosian, A., Tobias, B. C., Ceko, M., Kragel, P. A., Reis, F. M. C. V., Ji, S., Sehgal, M., Maesta-Pereira, S., Chakerian, M., Silva, A. J., Canteras, N. S., Wager, T., Kao, J. C., Adhikari, A. Dorsal premammillary projection to periaqueductal gray controls escape vigor from innate and conditioned threats. *eLife* (2021). doi: 10.7554/eLife.69178.

Wang, W.*, Schuette, P. J.*, Nagai, J., Tobias, B. C., Reis, F. M. C. V., Ji, S., de Lima, M. A. X., **La-Vu, M.**, Maesta-Pereira, S., Chakerian, M., Leonard, S. J., Lin, L., Severino, A. L., Cahill, C. M., Canteras, N. S., Khakh, B. S., Kao, J. C., Adhikari, A. Coordination of escape and spatial navigation circuits orchestrate versatile flight from threats. *Neuron* (2021). doi.org/10.1016/j.neuron.2021.03.033

Reis. F. M. C. V., Lee, J. Y., Maesta-Pereira, S., Schuette, P. J., Chakerian, M., Liu, J., **La-Vu, M.,** Tobias, B. C., Ikebara, J. M., Kihara, A. H., Canteras, N. S., Kao, J. C., Adhikari, A., Dorsal Periaqueductal gray ensembles represent approach and avoidance states. *eLife* (2021). doi.org/10.7554/eLife.64934

Sparse genetically-defined neurons refine canonical periaqueductal gray columnar organization

Abstract

When encountering external threats, survival depends on the engagement of appropriate defensive reactions to minimize harm. There are major clinical implications for identifying the neural circuitry and activation patterns that produce such defensive reactions, as maladaptive overactivation of these circuits underlies pathological human anxiety and fear responses. A compelling body of work has linked activation of large glutamatergic neuronal populations in the midbrain periaqueductal gray (PAG) to defensive reactions such as freezing, flight and threat-induced analgesia. These pioneering data have firmly established that the overarching functional organization axis of the PAG is along anatomically-defined columnar boundaries. Accordingly, broad activation of the dorsolateral column induces flight, while activation of the lateral or ventrolateral (l and vl) columns induces freezing. However, the PAG contains a diverse arrangement of cell types that vary in neurochemical profile and location. How these cell types contribute to defensive responses remains largely unknown, indicating that targeting sparse, genetically-defined populations can lead to a deeper understanding of how the PAG generates a wide array of behaviors. Though several prior works showed that broad excitation of the lPAG or vlPAG causes freezing, we found in mice that activation of lateral and ventrolateral PAG (l/vlPAG) cholecystokinin-expressing (cck) cells selectively caused flight to safer regions within an environment. Furthermore, inhibition of l/vlPAG-cck cells reduced avoidance of a predatory threat without altering other defensive behaviors like freezing. Lastly, l/vlPAG-cck activity decreased when approaching threat and increased during movement to safer locations. Taken together, these data suggest cck cells are driving threat avoidance states, which are epochs during which mice increase distance from threat and perform evasive escape. In contrast,

activating l/vlPAG cells pan-neuronally promoted freezing and these cells were activated near threat. These data underscore the importance of investigating genetically-identified PAG cells. Using this approach, we found a sparse population of cck-expressing l/vlPAG cells that have distinct and opposing function and neural activation motifs compared to the broader local ensemble defined solely by columnar anatomical boundaries. Thus, in addition to the anatomical columnar architecture of the PAG, the molecular identity of PAG cells may confer an additional axis of functional organization, revealing unexplored functional heterogeneity.

Introduction

The midbrain periaqueductal gray (PAG) has been implicated in numerous functions including pain modulation, vocalization, breathing, heart rate, hunting, freezing, and flight (Behbehani, 1995; Keay and Bandler, 2015; Motta et al., 2017; Silva and McNaughton, 2019). For decades, a great deal of effort has been put toward understanding how columnar subdivisions of the PAG control or contribute to distinct defensive behaviors (Bandler et al., 1985; Bandler and Carrive, 1988; Bandler and Shipley, 1994; Carrive, 1993; de Andrade Rufino et al., 2019; Gross and Canteras, 2012; Leman et al., 2003; Morgan and Clayton, 2005; Tomaz et al., 1988; Walker and Carrive, 2003; Zhang et al., 1990). Prior work indicates that the ventrolateral (vl) PAG column is necessary for conditioned freezing (Tovote et al., 2016). Though less studied than the vlPAG, optogenetic and electrical excitation of the lateral (l) PAG column also produces freezing (Assareh et al., 2016; Bittencourt et al., 2005, 2004; Yu et al., 2021). The dorsolateral (dl) PAG has a key role in controlling innate defensive behaviors. Indeed, dlPAG cells encode numerous defense behaviors including freezing, escape and risk-assessment (Del-Ben and Graeff, 2009; Deng et al., 2016; F. M. Reis et al., 2021; F. M. C. V. Reis et al., 2021), and activation of glutamatergic vGlut2+ dlPAG cells induces escape (Evans et al., 2018; Tovote et al., 2016). More recent work employing methods with genetic specificity

have focused on large PAG populations positive for broadly expressed markers such as Vgat, Vglut2 or CaMKIIa. For example, optogenetic activation of PAG neurons expressing CaMKIIa, which is ubiquitous in the region, elicited both freezing and flight (Deng et al., 2016). Though these findings provided important insights, they leave open the question of whether sparser PAG populations might control and encode more specific behavioral metrics.

Indeed, the PAG contains a diverse array of sparse cell types (Keay and Bandler, 2015; Silva and McNaughton, 2019; Yin et al., 2014). These cell types exhibit different neurochemical profiles and vary in anatomical location, often spanning more than a single column (Silva and McNaughton, 2019). For example, substance P-producing Tac1+ cells and enkephalin-releasing Penk+ cells are concentrated in dorsomedial and ventrolateral posterior PAG, while somatostatin-expressing cells can be found in dorsomedial and lateral columns (Allen Brain Atlas 2021; (Silva and McNaughton, 2019). It is possible that distinct cell types contribute to specific phenotypes controlled by the PAG. Accordingly, genetically-identified populations have been more deeply studied in other regions such as the lateral hypothalamus (Li et al., 2018) or the central amygdala (Fadok et al., 2017), leading to unprecedented insights on their function. However, cell-type specific dissections of sparse PAG populations remain scarce, and the functions of specific molecularly-defined cell populations are largely uncharacterized.

One population of interest is composed of cholecystokinin-releasing PAG (PAG-cck) cells (Allen Brain Atlas 2021). Intriguingly, intra-PAG infusion of cck in rats induces defensive behaviors and potentiates one-way escape behavior (Netto and Guimarães, 2004; Zanoveli et al., 2004). Additionally, cck excites PAG neurons at both pre- and postsynaptic loci (Liu et al., 1994; Yang et al., 2006), suggesting PAG-cck cells may have widespread effects on local cell

activity dynamics. However, despite these tantalizing results, to date PAG-cck cells have not been directly studied and their function remains unknown.

Here, we specifically target, manipulate and monitor the neural activity of PAG-cck cells. We show that lateral and ventrolateral (l/vl) PAG-cck cells are a small subset of glutamatergic cells, and that they selectively control flight to a safe location within an environment without affecting other defensive behaviors such as freezing or other l/vlPAG-mediated processes such as analgesia. Furthermore, though decades of prior work has consistently shown that PAG cells are activated by proximity to danger (Aguiar and Guimarães, 2009; Canteras and Goto, 1999; Deng et al., 2016; Evans et al., 2018; Mobbs et al., 2010, 2007; Watson et al., 2016), we find that l/vlPAG-cck cells are more active far from threat. In contrast, pan-neuronal activation of cells in the same l/vlPAG region induced freezing, and these cells closely encoded threat proximity and escape initiation. Thus we show that characterization of sparser, genetically-defined PAG populations may reveal cells that have unique functional roles and that may even show opposing patterns of neural activation relative to the broader local ensemble. Deciphering how molecularly-defined PAG populations complement and interact with the well-established anatomical columnar functional framework is a key step in understanding how this ancient structure controls a constellation of vital behaviors.

Results

cck+ cells comprise a sparse glutamatergic subset of l/vlPAG neurons.

The neuropeptide cck is expressed primarily in two clusters within the PAG: one located in the dorsomedial column and one spanning both the lateral and ventrolateral columns (Allen Brain Atlas 2021). Here, we focused on the latter population, which is more prevalent in the posterior than anterior PAG. To quantify the proportion of cck+ neurons in the posterior l/vlPAG

column, we used cre-dependent viral vectors to express GFP in cck+ cells of cck-ires-cre mice. We then immunostained posterior PAG slices against the pan-neuronal marker NeuN and quantified Neun/GFP overlap (Figure 1A). We observed GFP expression in the lPAG and vlPAG, but GFP expression was largely absent in the dlPAG (Figure 1A-B). Quantification showed that cck-GFP cells comprise approximately 5% of l/vlPAG neurons and are more prevalent in the l/vlPAG than dlPAG (Figure 1C; n=4, $t(3) = 8.743$, $p=0.0032$). Cholecystokinin-expressing cells in several brain regions such as cortex, hippocampus and amygdala are reported to be inhibitory (Kepecs and Fishell, 2014; Mascagni and McDonald, 2003; Nguyen et al., 2020; Whissell et al., 2015), though glutamatergic cck+ cells have also been reported in other regions (Wang et al., 2021). To determine if these cells are glutamatergic, we immunostained against the glutamatergic marker vGlut2 in PAG slices containing GFP-expressing cck+ cells (Figure 1D). We found a small fraction (9.6%) of vGlut2-labeled cells were also GFP-labeled (Figure 1E). Similarly, in situ hybridizations revealed that 8.58% of vGlut2-expressing cells co-express cck (Figure 9). Notably, we found that a majority of GFP-labeled cells (94.8%) were also vGlut2-labeled (Figure 1F). Our characterization shows that cck+ cells comprise a small, sparse subset of PAG neurons that span the lateral and the ventrolateral columns and are primarily glutamatergic.

l/vlPAG-cck stimulation induces a repertoire of behaviors distinct from pan-neuronal dlPAG and l/vlPAG stimulation

To study how various PAG populations may participate in distinct defensive phenotypes, we used an optogenetic approach to manipulate three different PAG subpopulations: pan-neuronal synapsin (syn)-expressing dorsolateral PAG neurons (dlPAG-syn), pan-neuronal syn-expressing lateral/ventrolateral PAG neurons (l/vlPAG-syn) and cholecystokinin-expressing lateral/ventrolateral PAG neurons (l/vlPAG-cck). We targeted these populations by local

injection of adeno-associated viruses (AAVs) delivering channelrhodopsin-2 (ChR2) coupled to a yellow fluorescent protein (YFP) tag into the dlPAG or l/vlPAG of wildtype (WT) mice and l/vlPAG of cck-ires-cre mice (Figure 2A-B, Figure 10). Mice injected with AAVs containing only YFP served as controls. The viral strategy used to transfect pan-neuronal l/vlPAG cells was synapsin-specific and did not exclude transfection of cck+ cells. We first optogenetically manipulated naive mice in an open field (Figure 2C-G). Activation of dlPAG-syn cells increased speed and open field corner entries compared to control mice (Figure 2H,L; dlPAG-eYFP, n=5; dlPAG-ChR2, n=4; speed: $t(7) = 2.495$, $p=0.0413$; corner entries: $t(7) = 2.451$, $p=0.044$). Notably, activation of only this, but not other PAG populations, induced escape jumping (Figure 2I; dlPAG-YFP, n=5; dlPAG-ChR2, n=4; $t(7) = 6.111$, $p=0.0005$). Light activation of l/vlPAG-syn cells strongly promoted freezing, and consequently reduced speed and corner entries (Figure 2H,J,L; (l/vlPAG-syn-eYFP, n = 5; l/vlPAG-syn-ChR2, n = 5; freezing: $t(8) = 9.176$, $p<0.0001$; speed: $t(8) = 7.741$, $p<0.0001$; corner entries: $t(8) = 4.548$, $p=0.0019$). Finally, we observed that activation of l/vlPAG-cck cells increased speed, reduced time spent in the open field center, and increased corner entries (Figure 2H,K-L; l/vlPAG-cck-eYFP, n = 17; l/vlPAG-cck-ChR2, n = 14; speed: $t(29) = 3.667$, $p=0.001$; center time: $t(29) = 3.334$, $p=0.0023$; corner entries: $t(29) = 5.253$, $p<0.0001$). Interestingly, activation of only this population increased time spent in the corners of the open field (Figure 2M; l/vlPAG-cck-eYFP, n = 17; l/vlPAG-cck-ChR2, n = 14; $t(29) = 2.967$, $p=0.006$). These results demonstrate that increased activity in these three PAG subpopulations elicited diverse behavioral phenotypes. Stimulation of l/vlPAG-cck cells induced a repertoire of behaviors distinct from pan-neuronal l/vlPAG and dlPAG activation. Furthermore, l/vlPAG-cck activation induced a preference for the corners of the open field, which represent the safest area in the arena as they allow mice to best limit visual detection by predators (La-Vu et al., 2020).

l/vlPAG-cck stimulation prompts entry into a dark burrow

We aimed to further investigate the exhibited preference for safety upon activation of l/vlPAG-cck cells. We developed the Latency to Enter (LTE) assay, a novel paradigm that measures flight to the safest region within an environment. The LTE is a square arena illuminated to 80 lux and contains a dark burrow (2 lux) in one corner. Mice were habituated to the arena for 10 min. To verify that mice perceived the burrow as a safer area within the assay, only mice that exhibited a preference for the burrow over the other three corners during habituation continued to Test on the following day (91.3%; 63 of 69 mice showed burrow preference). During Test, mice were placed in the LTE for a 1-min context reminder prior to ten consecutive trials. For optogenetic manipulation within the LTE, light delivery was alternated across the ten trials, beginning with a light-off trial. Prior to the start of each trial, mice were confined to the corner opposite of the burrow, the holding zone, with a transparent barrier for 15 sec. For light-on trials, light was delivered for the last 5 sec of the 15-sec period in the holding zone and continued until the end of the trial. The start of a trial (after 15 secs in holding zone) was marked by barrier removal and the trial ended upon burrow entry or 60 sec had passed. If a mouse entered the burrow, they could remain in the burrow for 10 sec prior to being returned to the holding zone. If they did not enter, they were immediately returned to the holding zone. The LTE allows assessment of the latency to enter a burrow from a fixed start location within an arena and enables structured sampling that is not dependent on mice traversing to a start location to initiate a trial, minimizing variability in inter-trial intervals.

To study if activation of PAG subpopulations can bias mice to flee to the burrow, we optogenetically manipulated dlPAG, l/vlPAG, and l/vlPAG-cck neurons in the Latency to Enter assay (Figure 3A-B). Despite similar levels of preference for the burrow during habituation, only optogenetic activation of l/vlPAG-cck neurons reduced latency to enter the burrow relative to YFP control mice (Figure 3C-F; l/vlPAG-cck-eYFP, n = 17; l/vlPAG-cck-ChR2, n = 14; t(29) =

4.108, p=0.0003). Notably, activation of syn-expressing l/vlPAG neurons robustly increased latency, as l/vlPAG-syn-ChR2 mice displayed substantial freezing with light-delivery compared to YFP mice (Figure 3F; l/vlPAG-syn-eYFP, n = 5; l/vlPAG-syn-ChR2, n = 5; t(8) = 3.777, p=0.0054). These data demonstrate increased activity in l/vlPAG-cck neurons can induce urgent flight to a safe burrow in a low-threat environment, a feature distinct from pan-neuronal l/vlPAG and dlPAG cells.

l/vlPAG-cck stimulation is aversive and anxiogenic, and can induce a hallmark sympathetic response

As there are no reports of genetically-targeted manipulation of l/vlPAG-cck cells, we sought to further characterize the behavioral phenotype induced by l/vlPAG-cck activation. We assessed the effects of optogenetic activation in mice expressing ChR2 in l/vlPAG-cck cells compared to YFP controls in anxiety and defense-related assays. Pairing light activation of l/vlPAG-cck cells with one of two chambers in the real-time place test assay resulted in avoidance of the stimulated chamber, suggesting increased l/vlPAG-cck activity is aversive (Figure 4A-C; eYFP, n = 14; ChR2, n = 8; t(20) = 4.938, p<0.0001). Furthermore, stimulation of l/vlPAG-cck cells in the elevated plus maze (EPM) reduced time spent in the open arms of the maze (Figure 4D-F; eYFP, n = 16; ChR2, n = 10; t(24) = 3.391, p=0.0024). A majority of laser onsets of the fixed duration stimulation protocol occurred while ChR2 mice occupied a closed arm (60.0 ± 10.0%, n=10); the same mice spent a majority of stimulation epochs in a closed arm (68.16 ± 3.39%), excluding the possibility that arm occupancy at laser onset may result in aversion of said arm. Light activation of l/vlPAG-cck cells also markedly increased pupil size, a hallmark sympathetic response (Figure 4G-H; eYFP, n = 4; ChR2, n = 7; t(9) = 2.908, p=0.0174). Pupil size measurements were carried out at a lower laser intensity (1.5mW versus 3.5mW in behavioral experiments) to avoid overt motor changes during head fixation as well as

movement-related arousal or stress that may have confounded measurements. Together, these results suggest l/vlPAG-cck cell activation is aversive, anxiogenic, and may elicit sympathetic activation.

l/vlPAG-cck inhibition delays entry into a dark burrow

Our data show that activation of l/vlPAG-cck neurons is sufficient to drive flight to safety (Figure 3). To determine if these neurons serve a critical role in these conditions, we next used AAV-mediated, cre-dependent bilateral expression of the inhibitory opsin archaerhodopsin (Arch) in cck-ires-cre mice to optically suppress activity of l/vlPAG-cck cells in the Latency to Enter assay (LTE, Figure 5A-B, Figure 11). During Test, green light (562-nm, constant) was delivered to the l/vlPAG in alternating trials and the latency to enter the burrow was measured at the end of each trial (Figure 5B). Though burrow preference was similar across both groups during habituation, light inhibition of l/vlPAG-cck cells increased latency to enter the burrow in Arch mice compared to eGFP control mice (Figure 5C-F; GFP, n = 6; Arch, n = 7; $t(11) = 2.447$, $p=0.0324$). Thus, in addition to our activation studies, we show activity in l/vlPAG-cck cells can bidirectionally control flight to a dark burrow under low-threat conditions.

l/vlPAG-cck stimulation increases avoidance of a live predator

Our data show that l/vlPAG activity is sufficient and necessary for flight to safety in the LTE, a low-threat environment in which perceived danger is diffuse and uncertain (La-Vu et al., 2020). However, it is still unknown if the l/vlPAG-cck population is involved in flight to safety in the presence of a well-defined, proximal threat such as a live predator.

To address this question, we optogenetically activated l/vlPAG-cck cells while introducing mice to Live Predator Exposure (Figure 6A). In this assay, mice are placed in an elongated rectangular arena that contains an awake rat restrained to one end by a harness

(Wang et al. 2021; Reis et al. 2021; Wang et al. 2021). Rats are natural predators of mice and mice exhibit robust defensive reactions during exposure to a live rat but not a similarly-shaped toy rat such as increased freezing, increased distance from the live rat, and reduced time in the zone containing the live rat (Figure 6B; n = 10; freezing: $t(9) = 3.519$, $p=0.0065$; threat distance: $t(9) = 13.09$, $p<0.0001$; threat zone: $t(9) = 7.604$, $p<0.0001$; (Wang et al., 2021). As the chamber does not contain a barrier and mice can freely roam the entire arena, Live Predator Exposure elicits a naturalistic and diverse repertoire of defensive responses (F. M. Reis et al., 2021; Wang et al., 2021).

We hypothesized that activation of l/vlPAG-cck cells in the presence of a live predator would exacerbate avoidance of the threat. To test this hypothesis, we delivered blue light (473-nm, 5-ms, 20-Hz) to the l/vlPAG of mice expressing YFP or ChR2-YFP in cck+ cells during live predator exposure (Figure 6C). Light was delivered in alternating 2-min epochs (Figure 6D-E). Light activation of cck+ cells reduced time spent in the threat zone and increased distance from the live rat (Figure 6F-G; eYFP, n = 10; ChR2, n = 9; time in threat zone: $t(17) = 3.808$, $p=0.0014$; distance: $t(17) = 3.24$, $p=0.0048$). Mice exhibit increased stretch-attend postures during exposure to predatory rats (Wang et al., 2021). This measure was reduced as a result of optogenetic activation, demonstrating that not all defensive behaviors are promoted by cck+ cell activation (Figure 6I; eYFP, n = 10; ChR2, n = 9; $t(17) = 2.441$, $p=0.0259$). Optogenetic activation of cck+ cells also induced a trend toward reduced number of approaches toward the rat, and did not alter freezing or locomotion (Figure 6H, J-K; eYFP, n = 10; ChR2, n = 9; approaches: $t(17) = 1.965$, $p=0.066$; freezing: $t(17) = 0.4696$, $p=0.6446$; locomotion: $t(17) = 1.682$, $p=0.1109$). Escape velocity can be an informative measure of threat avoidance; however, ChR2 mice did not exhibit enough escapes during light activation to compute this measure as they did not consistently approach the rat (see representative exploration track in Figure 6E, bottom row), which decreased escapes from the rat as escapes cannot occur without prior

approach. These results demonstrate activation of l/vlPAG-cck cells selectively enhanced avoidance of a live predator without altering freezing.

Importantly, these same results were not observed with cck+ activation during exposure to a control toy rat (Figure 12). Activating cck+ cells in this condition induced the same type of thigmotaxis seen during cck+ activation in an open field (Figure 2G). In the presence of the toy rat, thigmotaxis was uniformly induced throughout the environment periphery, both near and far away from the toy rat (see representative exploration track in Figure 12A). Thus, in the presence of the toy rat, cck+ activation induced avoidance of open spaces, rather than avoidance of the toy rat. In contrast, in the presence of the rat, activation of cck+ cells induced thigmotaxis only in the corners furthest away from the live rat (Figure 6E). These data show that l/vlPAG-cck cell activation increases avoidance of a live predator, but not of a control safe toy rat, showing that these cells may serve to minimize threat exposure by directing exploration towards safer regions within an environment.

l/vlPAG-cck inhibition reduces avoidance of a live predator

To evaluate the necessity of l/vlPAG-cck cells for threat avoidance in a high-threat environment, we bilaterally expressed cre-dependent inhibitory hM4di-mCherry in the l/vlPAG of cck-ires-cre mice to chemogenetically inhibit cck+ cells during live predator exposure (Figure 7A, Figure 13A). Mice expressing mCherry alone served as controls. A chemogenetic approach in this setting was beneficial because it enabled neuronal inhibition across a 10-min exposure without constant laser delivery, as prolonged laser stimulation may induce tissue heating, among other issues (Stujenske et al., 2015). Both hM4di and mCherry-only mice were injected with clozapine-N-oxide (CNO) or saline prior to two exposures to a toy rat and two exposures to an awake, live rat on separate, sequential days (Figure 7B-C). Injections occurred 40 min prior to exposure and the order of drug delivery was counterbalanced across groups. All metrics were

calculated as behavior exhibited following saline administration subtracted from behavior exhibited following CNO administration (CNO - SAL).

We found that l/vlPAG-cck inhibition significantly increased time spent in the threat zone, increased the number of approaches toward the rat, and reduced escape velocity from the rat (Figure 7D, F, H; threat zone: mCherry, n = 8; hM4Di, n = 12; t(18) = 2.554, p = 0.0199; approaches: mCherry, n = 8; hM4Di, n = 12; t(18) = 2.194, p=0.0496; escape velocity: mCherry, n = 7; hM4Di, n = 11; t(16) = 2.197, p = 0.0431). Cck+ inhibition also induced a trend towards decreased distance from the rat (Figure 7E; mCherry, n = 8; hM4Di, n = 12; t(18) = 1.937, p=0.0686). Inhibition did not alter approach velocity, stretch-attend postures, freezing, or distance traveled (Figure 7G,I-K).

Importantly, l/vlPAG-cck inhibition did not affect avoidance from a toy rat (Figure 13B-I), indicating effects of inhibition are specific to a live predator. Inhibition of cck cells also did not affect pain response latency during exposure to a heated plate assay (Figure 14), demonstrating that these cells do not affect other PAG functions such as analgesia (Samineni et al., 2017). Our data also show that inhibition of cck+ cells did not alter learning of auditory cued conditioned fear in the experimental conditions used (Figure 14). However, this negative result may be due to ceiling levels of freezing, and it is possible that these cells may have a role in fear learning employing different protocols. Together, these results show that, in addition to controlling avoidance measures under low-threat conditions, l/vlPAG-cck cells also selectively and bidirectionally control avoidance measures from a high-threat predator.

l/vlPAG-syn cells are more active near threat, while l/vlPAG-cck cells are more active far from threat

Numerous prior reports have consistently shown that PAG cells are activated by proximity to danger (Deng et al., 2016; Evans et al., 2018; Mobbs et al., 2010, 2007; F. M. Reis

et al., 2021; Watson et al., 2016). We next sought to observe endogenous l/vlPAG-cck activity under both low- and high-threat conditions. We performed in vivo fiber photometry recordings of synapsin and cck-expressing neurons in the l/vlPAG in the elevated plus maze (EPM) and live predator exposure assay (Figure 8A-C; Figure 15). These assays offer a safety gradient that allows us to assess how population activity is spatially modulated by threat proximity. Recording of syn-expressing l/vlPAG cells will inform whether activity patterns in cck-only population recordings are cell type-specific or region-specific.

We found that syn-GCaMP6f and cck-GCaMP6f activity were differentially modulated by EPM arms (Figure 8D). Specifically, mean df/F of l/vlPAG-syn cells increased after open-arm entry compared to closed-arm entry (Figure 8E; $n = 9$; $t(8) = 2.856$, $p=0.0213$). In contrast, cck activity was greater following closed-arm entry compared to open-arm entry (Figure 8F; $n = 11$; $t(10) = 2.561$, $p=0.0283$). Thus, in the low-threat EPM, l/vlPAG-cck activity diverged from broader l/vlPAG activity.

To determine if this feature might extend to a high-threat situation, we next performed photometry recordings of l/vlPAG pan-neuronal and cck-only populations during live rat exposure (Figure 8G). Mean df/F within spatial bins of varying distances from the safe wall shows syn-GCaMP6f activity was not differentially modulated when approaching the rat but significantly altered during escapes, with dF/F peaked when mice were most proximal to the predator and sharply reduced as mice gained distance from the predator (Figure 8H; approach: $r(8) = -0.255$, $p=0.476$; escape: $r(8) = 0.932$, $p<0.0001$). This pattern is consistent with previous reports coupling increased PAG activity with threat proximity and escape initiation (Deng et al., 2016; Evans et al., 2018; Reis et al., 2021; Watson et al., 2016).

Conversely, in cck-GCaMP6f mice, population activity was modulated during both approaches and escapes. cck+ activity ramped down as mice moved closer to the rat and

ramped up as mice escaped away from the rat (Figure 8I; approach: $r(8) = -0.792$, $p=0.006$; escape: $r(8) = -0.703$, $p=0.023$).

Syn-GCaMP6f activity was tightly time-locked with escapes, increasing prior to and peaking soon after escape initiation. cck+ activity also increased prior to escape but exhibited sustained heightened activity post-escape onset (Figure 8J-K). Our optogenetic experiments showed that increasing activity in l/vlPAG-syn cells robustly induced freezing; however we did not observe increased syn-GCaMP6f activity related to freeze bouts during predator exposure (Figure 8J). Finally, syn-GCaMP6f activity was greater in the threat zone than safe zone (Figure 8L; $n = 9$; $t(8) = 4.375$, $p=0.0024$) while cck-GCaMP6f activity was decreased in the threat zone relative to the safe zone (Figure 8M; $n = 12$; $t(11) = 2.658$, $p=0.0223$).

Importantly, these effects were not due to a correlation between speed and df/F (Figure 16) and were not observed during exposure to a toy rat (Figure 17). Together, these results suggest that though the syn-expressing l/vlPAG population was particularly attuned to more threatening aspects of both the EPM and live predator exposure, cck population activity was negatively modulated by threat proximity and increased during escape movements away from threat.

Discussion

Our study identifies a small, sparse, genetically-defined subset of cells within the PAG, cholecystokinin-expressing neurons (cck+), that control avoidance of threat in multiple contexts.

Activation of l/vlPAG cck+ cells induced evasion of open spaces and a live predator, which are, respectively, low and high intensity threats. Conversely, inhibition of cck+ cells delayed entry into a dark burrow and increased time spent near a live predator, showing these cells bidirectionally control avoidance measures in both low and high-threat environments.

Importantly, our manipulations did not alter freezing in any condition, demonstrating a specific role for cck+ cells in escape and avoidance. Cck+ cells also display increased activity with greater threat avoidance in both the low-threat elevated plus maze and the high-threat predator exposure.

We show that these features are specific to cck+ cells and oppose the broader local ensemble, as pan-neuronal activation of the same lPAG and vlPAG region drove robust freezing (Figure 2J), and pan-neuronal activation patterns show increased activity with greater threat proximity (Figure 8L), consistent with prior reports (Assareh et al., 2016; Bittencourt et al., 2005; Deng et al., 2016; Evans et al., 2018; Mobbs et al., 2010, 2007; F. M. Reis et al., 2021; Tovote et al., 2016; Watson et al., 2016; Yu et al., 2021). Importantly, though our strategy of synapsin-specific transfection does not exclude cck+ cells, we show cck+ cells are a small, sparse population, making up only about 5% of l/vlPAG neurons (Figure 1), and are unlikely to be significantly driving fluorescence in pan-neuronal photometry recordings. Together, these data suggest that l/vlPAG cck+ cells are selectively driving and signaling a behavioral state of threat avoidance and diverges from pan-neuronal l/vlPAG function.

We also characterized the effect of l/vlPAG cck+ activation in pupil size, a physiological measure that is modulated by threat exposure (Wang et al., 2021). To do so, we used lower blue laser light intensity (1.5 mW for pupil measurements versus 3-3.5 mW in all behavioral experiments). This was in order to avoid escape attempts, which may result in damage and dislocation of the fiber optic cannula when mice try to escape while head-fixed. These data suggest that lower l/vlPAG cck+ stimulation is sufficient to produce a defensive state with physiological changes, while higher stimulation yields a more intense state than includes escapes, which are likely also accompanied by physiological changes.

One inconsistency in our findings is a lack of increase in pan-neuronal activity during freeze bouts in the predator assay (Figure 8), despite ChR2 activation of this population driving robust freezing in an open field (Figure 2) and Latency to Enter assay (Figure 3). This may be due to several factors including ChR2 activation may stimulate more ventral cells than are being recorded using fiber photometry. Another possibility is that ChR2 activation may drive activity in some few cells that are responsible for driving the robust freezing observed, and the fluorescence of these sparse cells were washed out in Ca2+ recordings. Finally, it is possible that l/vlPAG activity reflected complex population dynamics related to the heightened behavioral state induced by high-threat predator exposure, resulting in endogenous activity that is more complex than is elicited with artificial activation in a low-threat environment.

l/vlPAG cck cell activity may drive the threat avoidance behavioral state

It is noteworthy that in all assays used in this work, mice voluntarily chose when to avoid or approach threats, which consisted of either open spaces or a predator. Threat exposure is thus driven by internal state switches of threat approach and threat avoidance states (La-Vu et al., 2020; F. M. Reis et al., 2021). In the threat approach state, mice decrease distance to threats and perform risk-evaluation behaviors, such as stretch-attend postures. Conversely, in the threat avoidance state, mice stay away from threats and initiate evasive escape.

We show that l/vlPAG cck+ cells were active away from threats and and during evasion from threats. Furthermore, activity of these cells was sufficient and necessary for threat avoidance and escape. We thus propose that l/vlPAG cck+ cells are a key driver of the threat avoidance behavioral state. One intriguing question arising from this view is that if cck+ activity causes escape when the mouse is near threat, then why does increased cck+ activity in the

safe region not elicit escape when the mouse is away from threat as well? In other words, why did cck+ activity not render the safe region aversive, and thus cause escape from this safe location? When the mouse neared the rat, it was in the threat approach state, and thus cck+ activity was low. Immediately prior to escaping, the mouse switched to the threat avoidance state, and then escaped to the region far from the rat, and this action was accompanied by high cck+ activity which presumably drove the escape. However, cck+ activity remained high far from the rat in the safe zone. The 'safe region' in the rat assay was not truly danger-free, but was only safer in relation to the rat 'threat zone' (see scheme in Figure 6A). Even in the safe zone, it is likely that the mouse was motivated to further increase distance from the rat, as it was in the avoidance state, and this motivation may be related to the increased cck+ activity seen away from the rat. However, there was no better or safer place for the mouse to occupy in this assay, so it remained in the 'safe zone' even though this region was still more aversive and dangerous than would be ideal for the mouse. This was also seen in our ChR2 activation of cck+ cells during rat exposure, in which increased cck+ activity did not cause indiscriminate escape from the safe zone, but rather strong thigmotaxis between the two safest corners within the safe zone. Thus, cck+ activity did not cause escape from the safe zone because cck+ activity is not predictive of simply escaping away from the current location, but rather it may increase the motivation to escape to the safest region within the environment. Furthermore, optogenetic vl/lPAG cck inhibition increased time near the predator, further supporting the view that cck activity drives the threat avoidance state. Previously we reported distinct synapsin-expressing PAG ensembles that consistently encode both threat approach and threat avoidance states across different threat modalities, such as open spaces and predators (Reis et al., 2021). The current work suggests that cck+ cells may be a genetically-identified ensemble that promotes the threat avoidance state during exposure to these same stimuli.

Role of cck cells in the l/vlPAG

Long-standing evidence links increased PAG activity with higher threat exposure. Following predator exposure, the rodent PAG exhibits increased Fos expression (Aguiar and Guimarães, 2009; Canteras and Goto, 1999; Mendes-Gomes et al., 2020). Pharmacological blockade of NMDA receptors in the dorsal or ventrolateral PAG increased open arm exploration in the EPM (Guimarães et al., 1991; Molchanov and Guimarães, 2002). Single unit recordings show dPAG and vPAG units display significant increases in firing rate after exposure to cat odor (Watson et al., 2016). Moreover, the dPAG is sensitive to sensory aspects of threat distance and intensity, displaying increased activity with greater proximity to an awake predator (Deng et al., 2016). In humans, PAG activity is positively correlated with threat imminence (Mobbs et al., 2010, 2007). Within the dPAG, glutamatergic neurons are key for escape initiation and vigor, and dPAG flight-related cells exhibited prominent firing early during flight and declined as mice fled further from a predator (Deng et al., 2016; Evans et al., 2018).

Similarly to previous reports of the PAG (Assareh et al., 2016; Bittencourt et al., 2005; Tovote et al., 2016; Yu et al., 2021), we also observed higher pan-neuronal PAG activity during threat proximity. However, in contrast, cck+ activity was reduced with threat proximity. To our knowledge, this is the first PAG cell type identified in which endogenous activity is reduced with threat proximity.

Pan-neuronal optogenetic activation of l/vlPAG cells produced strong freezing (Figure 2J), in agreement with prior reports showing that electrical or optogenetic excitation of the lPAG or vlPAG produced freezing (Assareh et al., 2016; Bittencourt et al., 2005, 2004; Yu et al., 2021). Furthermore, activation of glutamatergic vlPAG neurons powerfully elicited freezing (Tovote et al., 2016). VLPAG lesions curtailed freezing during predator exposure and

conditioned fear (de Andrade Rufino et al., 2019; Fanselow et al., 1995). Taken together, a plethora of data link lPAG and vlPAG activation with freezing. The identification of l/vlPAG cck+ neurons as a population that drives escape, rather than freezing, thus opposes the canonical function of this region.

Prior data have suggested that the PAG participates in relaying aversive unconditioned stimulus information to the amygdala to inform associative plasticity, and this feature is critical to prediction error coding (Herry and Johansen, 2014; Johansen et al., 2010; McNally et al., 2011). Though studies have identified a role of vlPAG neurons in prediction error coding (Ozawa et al., 2017; Walker et al., 2020), our inhibition of cck+ cells during fear acquisition did not alter freezing during acquisition nor retrieval, suggesting that a role in prediction error coding may be carried out by other vlPAG cells. It is however possible that these cells have a role in controlling learned fear under other conditions that were not tested in this work. Our l/vlPAG activation studies reaffirm the lPAG and vlPAG roles in freezing and concurrently highlight the non-canonical role of cck+ cells in driving flight.

The PAG's role in flight has historically been attributed to the dorsal PAG. Dorsal PAG stimulation in rodents has been shown to induce marked escape responses such as explosive vertical jumping, running, aversion and panic-related sympathetic responses (Del-Ben and Graeff, 2009; Depaulis et al., 1992; Fanselow, 1991; Jenck et al., 1995; Perusini and Fanselow, 2015; Valenstein, 1965). The present findings suggest the role of the PAG in avoidance extends beyond the dorsal PAG column, in part, to the l/vlPAG. Interestingly, the flight pattern observed from l/vlPAG cck+ activation is characteristically different from escape canonically described in PAG studies, as they are void of robust protean vertical jumping seen in dlPAG activation in this study (Figure 2I) and prior work (Ullah et al., 2015). Therefore our work draws attention to two

distinct types of escape: flight to escape the environment as seen by jumps induced by pan-neuronal activation of dlPAG cells (Figure 2I) and flight to safer regions within the environment, as shown by l/vlPAG cck+ cell activation (Figure 2-3,6). Further studies are needed to identify how l/vlPAG cck+ cells affect downstream targets to produce escape, and also to investigate which inputs to these cells are necessary for activating them.

Complementing columnar functional organization

Columnar organization in the PAG is supported by functional and anatomical similarities along the rostrocaudal axis. Broad activation of the dorsolateral column induces flight, hypertension, and tachycardia, while activation of the ventrolateral column induces freezing, hypotension and bradycardia (Keay and Bandler, 2015). Neurotransmitter and receptor expression profiles and afferent/efferent connections are also generally (but not always) homogeneous within a single column along the anteroposterior axis (Silva and McNaughton, 2019).

However, to achieve a more complete understanding of PAG function, there may be other considerations in addition to columnar organization. There are exceptions to homogeneity along the anterior-posterior axis of columnar boundaries in PAG afferent and efferent connectivity. For example, adrenergic and noradrenergic medullary afferents preferentially target the rostral vlPAG and the central amygdala receives input from cells highly concentrated in the caudal but not rostral vlPAG (Silva and McNaughton, 2019). Furthermore, there are genetic markers that do not span an entire column; GABA-immunopositive cells are more prevalent in caudal than rostral cat vlPAG (Barbaresi, 2005). Tachykinin-1 (i.e., tac1), which is a marker of substance P-expressing cells, broadly spans multiple columns rostrally but concentrates in dorsolateral and ventrolateral columns caudally in the rat (Liu and Swenberg,

1988). Expression of rat endocannabinoid and glycine receptors also vary rostrocaudally, becoming more present in caudal PAG (Araki et al., 1988; Herkenham et al., 1991; Silva and McNaughton, 2019). It is likely that exploration of these genetically-defined PAG populations will reveal novel insights. Indeed, inhibition of lPAG VGAT and lPAG VGlut2+ neurons impair the chase and attack of prey, respectively (Yu et al., 2021), and glutamatergic vlPAG neurons project to the medulla to control freezing (Tovote et al., 2016). Moreover, l/vlPAG tac1+ cells have been shown to specifically control itching behavior (Gao et al., 2019), further supporting the value of investigating sparse genetically-defined PAG populations.

Recent work has shown that examination of genetic diversity can unveil deep and novel understanding even in well-studied regions such as the amygdala. Accordingly, work from numerous groups dissecting glutamatergic basolateral amygdala cells based on genetic markers and projection targets has revealed the region's complex control of anxiety and valence processing (Felix-Ortiz et al., 2013; Kim et al., 2016; Tye et al., 2011).

In this study, using a genetic approach, we uncovered a sufficient and critical role of cck+ cells in controlling threat avoidance. Cck-expressing cells are one among many largely uncharacterized genetically-defined populations in the PAG (Yin et al., 2014), and here we outline a framework to assess how a single cell type may contribute to the vast constellation of behaviors controlled by the PAG. These results highlight that the molecular identity of PAG cells can lend key insight into functional motifs that govern how the PAG produces defensive responses and may serve as an additional axis of functional organization, complementing the well-established anatomical columnar PAG divisions.

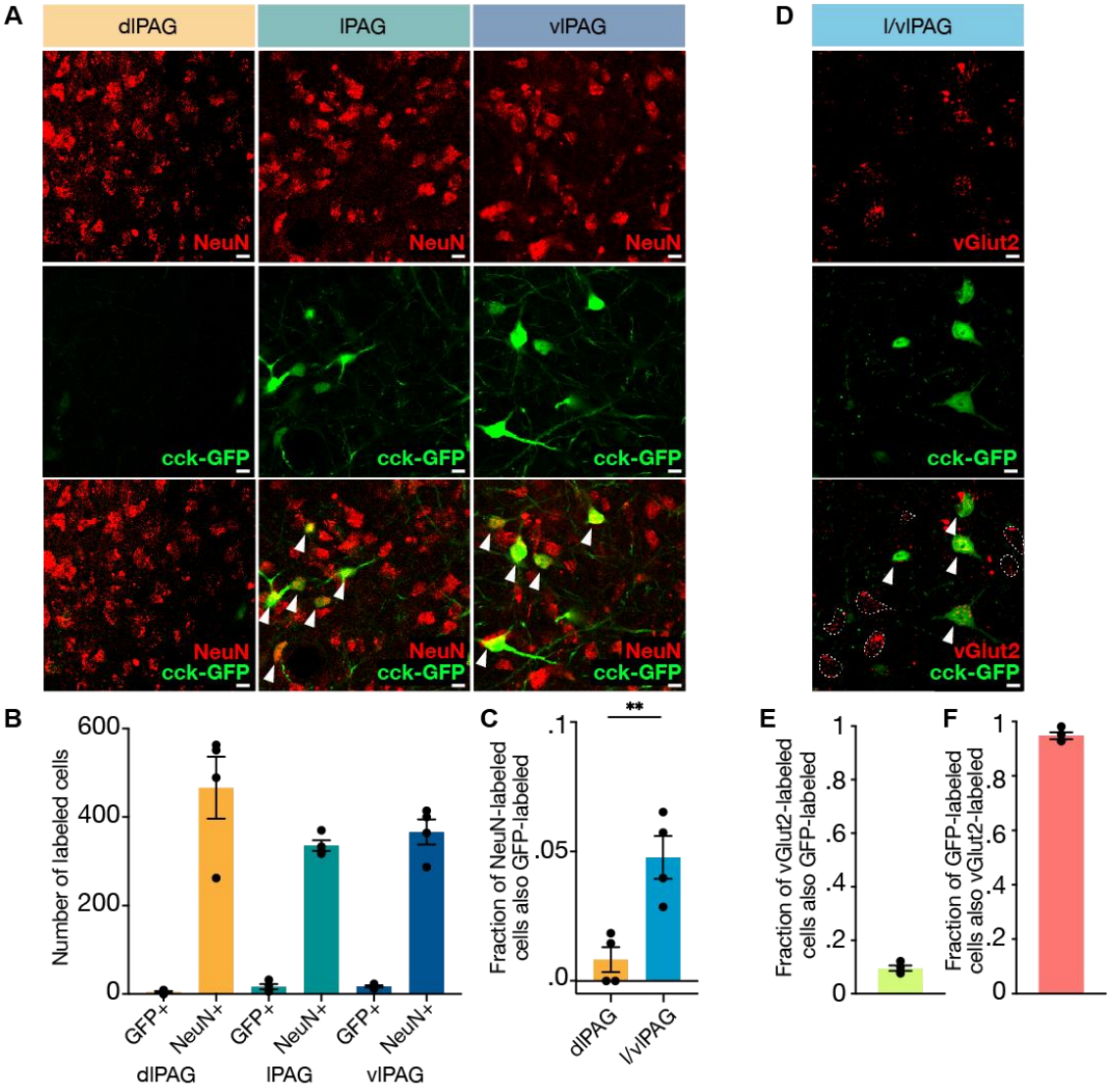

Figure 1. Cck+ cells comprise approximately 5% of l/vlPAG neurons and are primarily glutamatergic. (A) Example histology images showing immunostaining of pan-neuronal marker NeuN (top row), viral-mediated expression of GFP in cck-expressing cells (middle row), and overlay of NeuN and cck-GFP (bottom row) in the dorsolateral (left column), lateral (middle column), and ventrolateral (right column) PAG. Scale bars, 10μm. (B) Raw counts of cck-GFP+ and NeuN+ cells in the dlPAG, lPAG, and vlPAG. (C) Fraction of NeuN-labeled cells that are also GFP-labeled in the dlPAG and l/vlPAG. Cck-expressing cells comprise ~5% of l/vlPAG neurons and constitute significantly more of l/vlPAG neurons than dlPAG neurons (n=4; paired t-test, **p=.0032). (D) Immunostaining of glutamatergic marker vGlut2 in cck cells. Example histology images showing vGlut2 (top), cck-GFP (middle) and vGlut2/GFP overlay (bottom). White arrow indicates vGlut2+/GFP+ cell. Dashed outline indicates vGlut2+/GFP- cell. Scale bar, 10μm. (E) 9.6% of vGlut2-labeled cells in the l/vlPAG are also GFP-labeled (n = 4; 302 vGlut2/GFP+ of 3115 vGlut2+ cells). (F) A majority (94.8%) of GFP-labeled cells in the l/vlPAG are also vGlut2-labeled (n = 4; 302 vGlut2+/GFP+ of 317 GFP+ cells). Mean ± SEM.

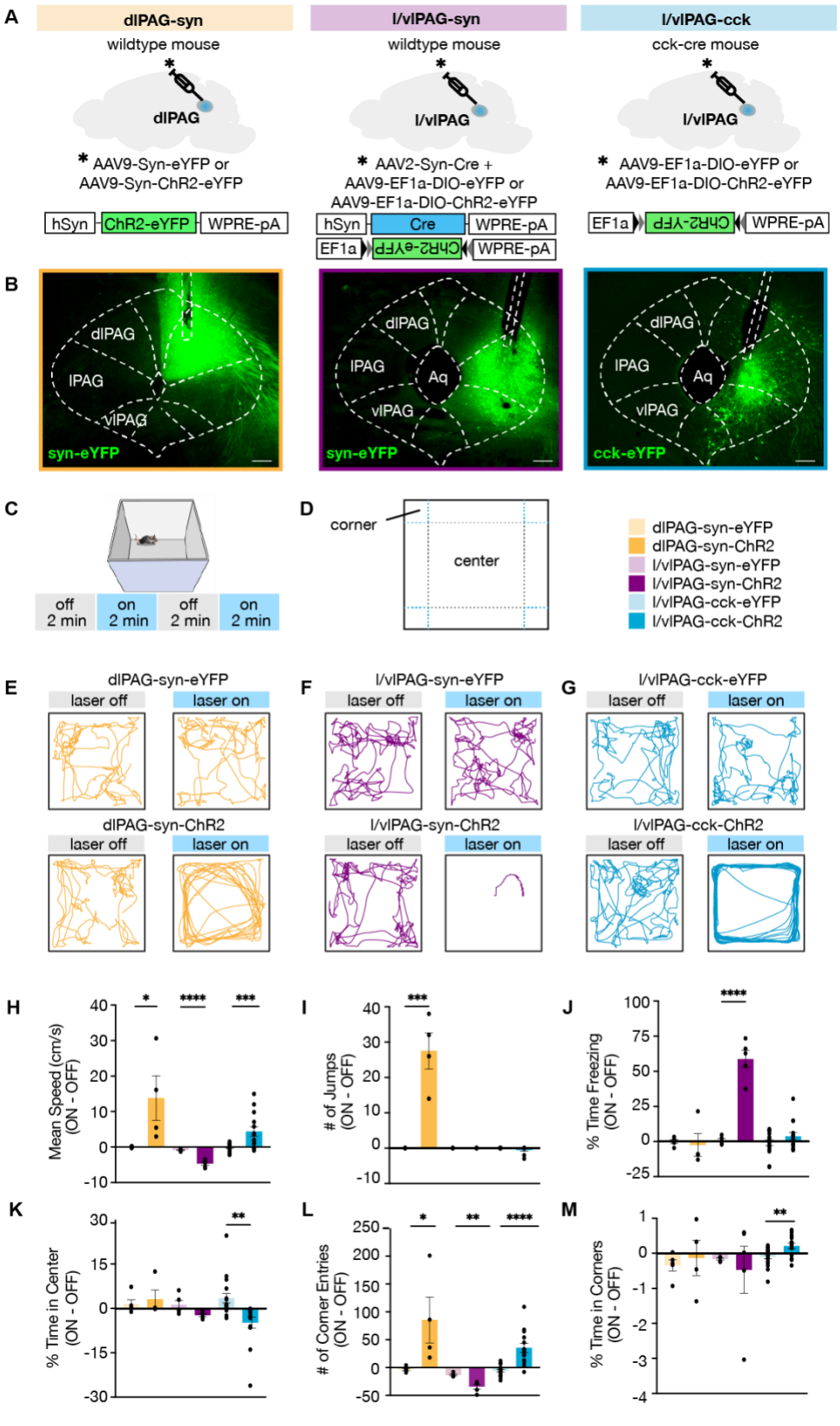
A
dlPAG-syn
wildtype mouse
dlPAG
* AAV9-Syn-eYFP or AAV9-Syn-ChR2-eYFP
hSyn
ChR2-eYFP
WPRE-pA
l/vlPAG-syn
wildtype mouse
l/vlPAG
* AAV2-Syn-Cre + AAV9-EF1a-DIO-eYFP or AAV9-EF1a-DIO-ChR2-eYFP
hSyn
Cre
WPRE-pA
EF1a
ChR2-eYFP
WPRE-pA
l/vlPAG-cck
cck-cre mouse
l/vlPAG
* AAV9-EF1a-DIO-eYFP or AAV9-EF1a-DIO-ChR2-eYFP
EF1a
ChR2-YFP
WPRE-pA
B
dlPAG
lPAG
vlPAG
Aq
syn-eYFP
cck-eYFP
C
off 2 min
on 2 min
off 2 min
on 2 min
D
corner
center
dlPAG-syn-eYFP
dlPAG-syn-ChR2
l/vlPAG-syn-eYFP
l/vlPAG-syn-ChR2
l/vlPAG-cck-eYFP
l/vlPAG-cck-ChR2
E
dlPAG-syn-eYFP
dlPAG-syn-ChR2
F
l/vlPAG-syn-eYFP
l/vlPAG-syn-ChR2
G
l/vlPAG-cck-eYFP
l/vlPAG-cck-ChR2
laser off
laser on
H
Mean Speed (cm/s) (ON - OFF)
I
# of Jumps (ON - OFF)
J
% Time Freezing (ON - OFF)
K
% Time in Center (ON - OFF)
L
# of Corner Entries (ON - OFF)
M
% Time in Corners (ON - OFF)

Figure 2. l/vlPAG-cck stimulation induced a repertoire of behaviors distinct from pan-neuronal l/vlPAG and dlPAG activation. (A) Viral strategy to express enhanced yellow fluorescent protein (eYFP) or light-sensitive channelrhodopsin (ChR2-eYFP) in synapsin-expressing cells in the dorsolateral periaqueductal gray (dlPAG-syn, left), synapsin-expressing cells in the lateral and ventrolateral PAG (l/vlPAG-syn, middle), and cholecystokinin-expressing cells in the lateral and ventrolateral PAG (l/vlPAG-cck, right). A fiber optic cannula was then implanted over respective regions. (B) Histology of eYFP expression in dlPAG-syn (left), l/vlPAG-syn (middle) and l/vlPAG-cck (right). Scale bar, 200µm. (C) Stimulation protocol in the Open Field. Blue light (473-nm, 5-ms, 20-Hz) was delivered in alternating 2-min epochs (OFF-ON-OFF-ON) for 8-min total. (D) Diagram indicating center and corners of the Open Field assay. (E-G) Example locomotion maps in the Open Field during laser-on and laser-off epochs of either mice expressing eYFP (top) or ChR2-eYFP (bottom) in dlPAG-syn (E), l/vlPAG-syn (F), and l/vlPAG-cck (G) populations. (H-M) Bars depict respective behaviors during light-off epochs subtracted from light-on epochs (ON minus OFF). Light delivery to dlPAG of syn-ChR2 mice increased mean speed, jumps and corner entries compared to dlPAG-syn-eYFP mice (dlPAG-eYFP, n = 5; dlPAG-ChR2, n = 4; unpaired t-tests; speed, *p=0.041; jumps, ***p=0.0005; corner entries, *p=0.044). Light delivery to the l/vlPAG of syn-ChR2 mice reduced mean speed, increased freezing, and reduced corner entries compared to l/vlPAG-syn-eYFP mice (l/vlPAG-syn-eYFP, n = 5; l/vlPAG-syn-ChR2, n = 5; unpaired t-tests; speed, ****p<0.0001; freezing, ****p<0.0001; corner entries, **p=0.0019). Light delivery to the l/vlPAG of cck-ChR2 mice increased mean speed and corner entries while reducing center time compared to l/vlPAG-cck-eYFP mice (l/vlPAG-cck-eYFP, n = 17; l/vlPAG-cck-ChR2, n = 14; unpaired t-tests; speed, ***p=0.001; corner entries, ****p<0.0001; center time, **p=0.0023). Importantly, time spent in corners increased during light delivery to l/vlPAG-cck-ChR2 mice compared to l/vlPAG-cck-eYFP mice (unpaired t-test, **p=0.006). Mean ± SEM.

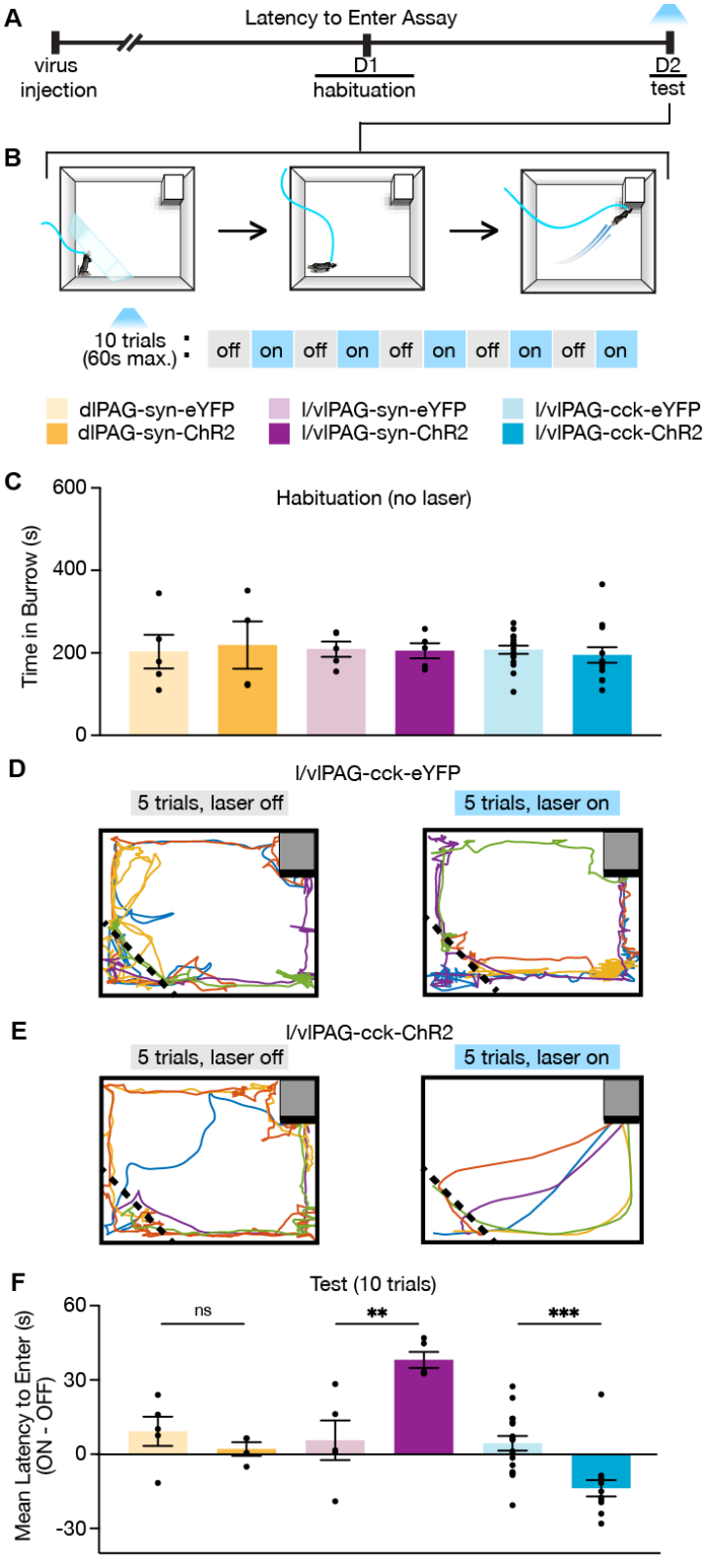
A
Latency to Enter Assay
virus injection
D1 habituation
D2 test
B
10 trials (60s max.):
off on off on off on off on off on
dlPAG-syn-eYFP
dlPAG-syn-ChR2
l/vlPAG-syn-eYFP
l/vlPAG-syn-ChR2
l/vlPAG-cck-eYFP
l/vlPAG-cck-ChR2
C
Habituation (no laser)
Time in Burrow (s)
600
400
200
0
D
l/vlPAG-cck-eYFP
5 trials, laser off
5 trials, laser on
E
l/vlPAG-cck-ChR2
5 trials, laser off
5 trials, laser on
F
Test (10 trials)
Mean Latency to Enter (s) (ON - OFF)
60
30
0
-30
ns
**
***

Figure 3. l/vlPAG-cck stimulation prompts entry into a dark burrow in the absence of threat, unlike pan-neuronal l/vlPAG and dlPAG stimulation. (A) Timeline of Latency to Enter assay. Mice were habituated to a chamber containing a dark burrow for 10-min 1-day prior to test. Mice with preference for burrow during habituation were included during Test. (B) Schematic of Latency to Enter assay during Test. Left: At the beginning of each trial, mice were confined to a corner opposite of a dark burrow with a transparent wall (holding zone). After 15 s, the transparent barrier is removed and mice can freely move about the chamber. The trial ends when mice enter the burrow or 60 s have passed. Blue light (473-nm, 5-ms, 20-Hz) is delivered in alternating trials. In light-on trials, blue light delivery begins 5-s prior to barrier removal. After burrow entry, mice can remain in the burrow for 10 s before being returned to the holding zone. (C) Bars represent average time spent in the burrow during a 10-min habituation (dlPAG: eYFP, n = 5; ChR2, n = 4; l/vlPAG-syn: eYFP, n = 5; ChR2, n = 5; l/vlPAG-cck: eYFP, n = 17, ChR2, n = 14). (D-E) Example locomotion map of 5 light-off (left) and 5 light-on trials (right) in a l/vlPAG-cck-eYFP mouse (D) and l/vlPAG-cck-ChR2 mouse (E). (F) Individual dots represent mean latency during 5 light-on epochs subtracted by mean latency during 5 light-off epochs (ON minus OFF). Trials without entry were regarded as latency of 61 s. Light delivery increased latency to enter the burrow in l/vlPAG-syn-ChR2 mice compared to l/vlPAG-syn-eYFP mice (l/vlPAG-syn-eYFP, n = 5; l/vlPAG-syn-ChR2, n = 5; unpaired t-test, **p=0.0054). Light delivery reduced latency to enter the burrow in l/vlPAG-cck-ChR2 mice compared to l/vlPAG-cck-YFP mice (l/vlPAG-cck-eYFP, n = 17; l/vlPAG-cck-ChR2, n = 14; unpaired t-test, ***p=0.0003). Stimulation of the dlPAG did not affect latency (dlPAG-eYFP, n = 5; dlPAG-ChR2, n = 4). Mean ± SEM.

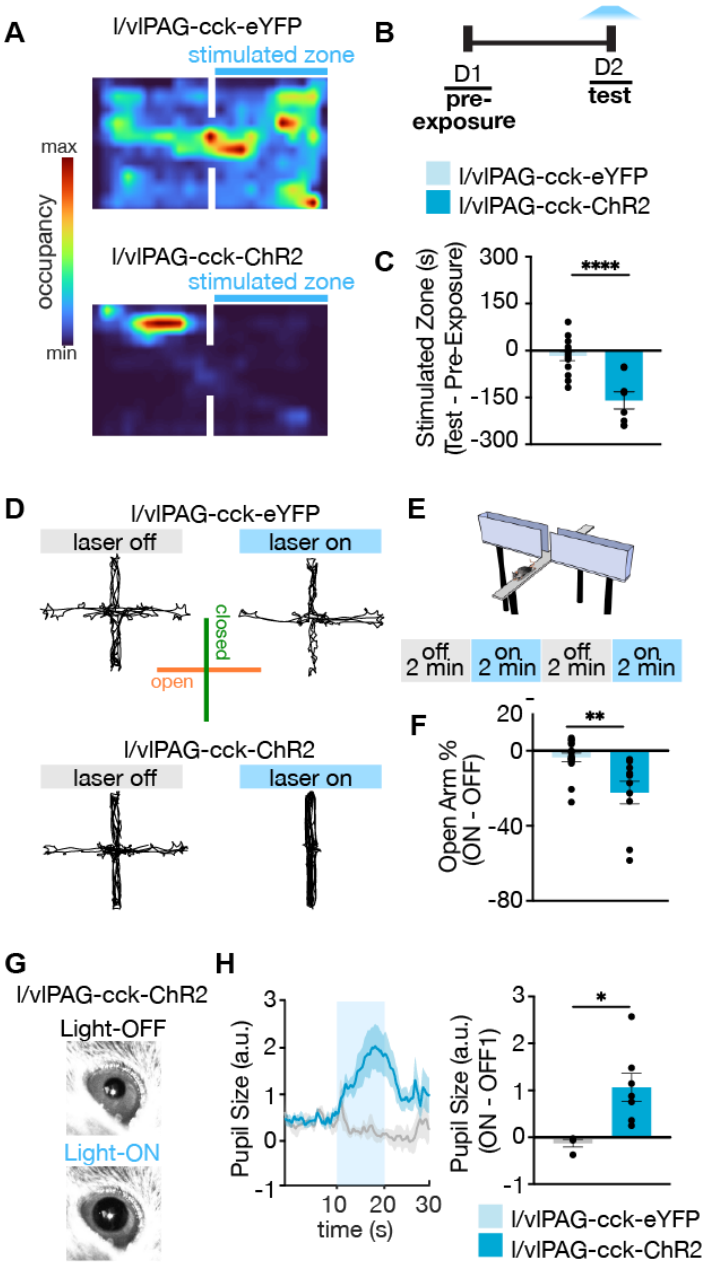

Figure 4. Further characterization of l/vlPAG-cck neurons demonstrates stimulation is aversive, anxiogenic, and induces hallmark sympathetic responses. (A) Example spatial map of real-time place test (RTPT) depicting min/max occupancy during Test of a l/vlPAG-cck-eYFP mouse (top) and l/vlPAG-cck-ChR2 mouse (bottom). Blue light delivery was paired with occupancy of one chamber in the RTPT during a 10 min Test. (B) Timeline for RTPT assay. Each session lasted 10 min. (C) Dots represent time spent in the stimulated zone during Test minus time spent in the same zone during Pre-Exposure (without light delivery). Bars are averaged across l/vlPAG-cck-eYFP and l/vlPAG-cck-ChR2 groups, respectively. Stimulation of l/vlPAG-cck neurons results in avoidance of stimulated zone, compared to control YFP group (eYFP, n = 14; ChR2, n = 8; unpaired t-test, ****p < 0.0001). (D) Example locomotion maps of l/vlPAG-cck-eYFP (top) and l/vlPAG-cck-ChR2 mice (bottom) during light-off (left) and light-on (right) epochs. (E) Stimulation protocol in elevated plus maze assay (EPM). (F) Dots represent percent of time spent in open arms during light-on epochs normalized by light-off epochs (ON minus OFF) of l/vlPAG-cck-eYFP or l/vlPAG-cck-ChR2 mice. Light delivery to ChR2 mice reduced open-arm occupancy relative to eYFP mice (eYFP, n = 16; ChR2, n = 10; unpaired t-test, **p=0.0024).(G) Example pupil images of a head-fixed l/vlPAG-cck-ChR2 mouse without (top) and with blue-light delivery (bottom). (H) Left: Average data showing pupil size during baseline, stimulation, and post-stimulation periods

(labeled OFF, ON, and OFF respectively). Each period lasted 10 sec. During stimulation, blue light was delivered to l/vlPAG. Right: Blue light delivery increased pupil size in l/vlPAG-cck-ChR2 compared to l/vlPAG-cck-eYFP mice (eYFP, n = 4; ChR2, n = 7; unpaired t-test, *p=0.0174). Mean ± SEM.

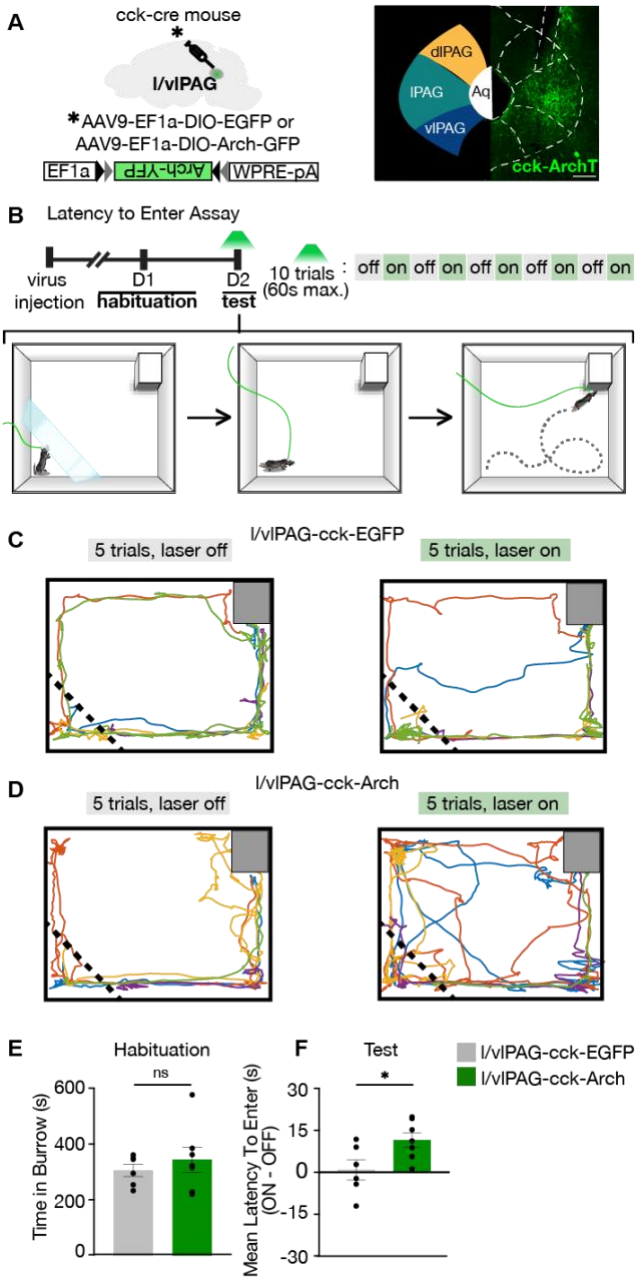

Figure 5. l/vlPAG-cck inhibition delays entry into a dark burrow. (A) Left: Strategy for viral expression of cre-dependent GFP or Arch-GFP in l/vlPAG of cck-cre mice. Right: Histology showing Arch-GFP expressed in cck+ cells in the l/vlPAG. Scale bar, 200µm. (B) Top: Timeline of Latency to Enter assay. Test consists of 10 trials, with green light delivery to l/vlPAG in alternating trials. Bottom: Schematic of assay during test. At the start of trial, mice were confined to a holding zone for 15s with a transparent barrier. When the barrier was removed, mice were free to explore the arena. Trial ended upon burrow entry or 60s have passed. (C) Example locomotion maps of five trials without (left) and with (right) green light delivery in l/vlPAG-cck-GFP mice. (D) Same as (C) but in l/vlPAG-cck-Arch mouse. (E) No difference in burrow occupancy during 10-min habituation between l/vlPAG-cck-GFP and l/vlPAG-cck-Arch mice (GFP, n = 6; Arch, n = 7; unpaired t-test). (F) Green light delivery to l/vlPAG increased latency to enter burrow in l/vlPAG-cck-Arch mice compared to l/vlPAG-cck-GFP mice. Each dot represents average latency during 5 light-on trials minus average latency of 5 light-off trials (GFP, n = 6; Arch, n = 7; unpaired t-test, *p=0.0324). Mean ± SEM.

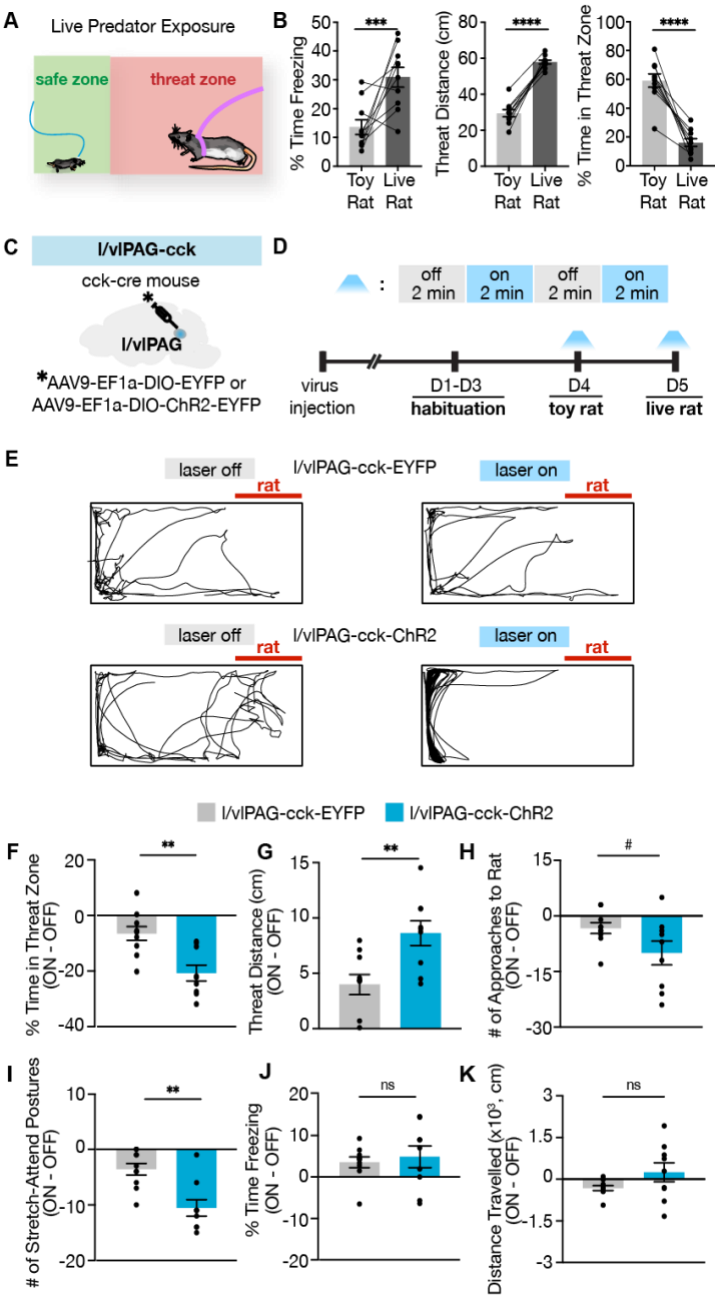

Figure 6. l/vlPAG-cck activation robustly enhances avoidance from a live predator without altering freezing. (A) Schematic of Live Predator Exposure assay. Mice are placed in a long rectangular chamber (70 x 25 x 30 cm) containing an awake rat restrained with a harness to one end. The chamber does not contain a barrier and mice can move freely. The area containing the rat is considered a 'threat zone' and the area furthest from the rat is considered a 'safe zone.' (B) Exposure to a live rat increased freezing and threat distance while reducing time in threat zone compared to exposure to a toy rat (n = 10, paired t-tests; freezing, ***p=0.0065; threat distance, ****p< 0.0001; time in threat zone, ****p< 0.0001). (C) EYFP or ChR2-eYFP was expressed in l/vlPAG-cck cells and a fiber-optic cannula was implanted over the l/vlPAG. (D) Timeline of Live Predator Assay. Blue light was delivered in alternating 2-min epochs during Toy Rat exposure and Live Rat exposure. (E) Example locomotion maps during laser-off (left) and laser-on (right) epochs of an eYFP mouse (top) and ChR2-eYFP mouse (bottom). (F-K) Optogenetic stimulation of l/vlPAG-cck cells reduced time in threat zone (F; eYFP, n = 10; ChR2, n = 9; unpaired t-test, **p=0.0014), increased threat distance (G, unpaired t-test, **p=0.0048), and reduced stretch-attend postures (I, unpaired t-test, **p=0.0012). Number of approaches to the rat trended toward significance (H, #p=0.066). Freezing (J) and distance travelled (K) were not significantly affected. Mean ± SEM.

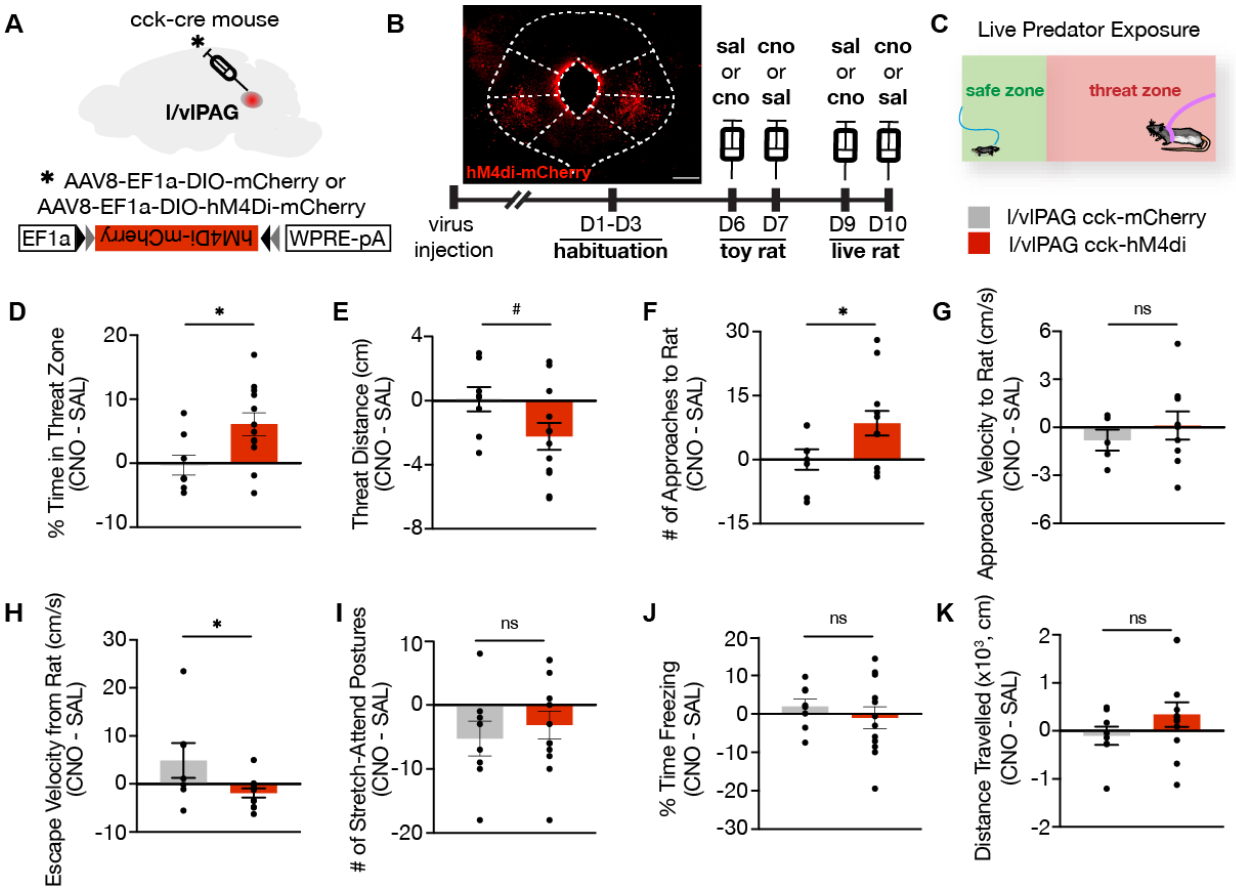

Figure 7. l/vlPAG-cck inhibition increases time spent near a live predator and reduces escape vigor without altering freezing. (A) Viral strategy for bilateral expression of inhibitory designer receptor hM4Di-mCherry or mCherry in cck cells in the l/vlPAG. (B) Top-left: Expression of hM4Di-mCherry in l/vlPAG-cck cells. Scale bar, 200µm. Bottom: Timeline for DREADD experiments. Saline or clozapine-N-oxide (CNO, 10mg/kg) occurred 40 min prior to exposure. (C) Live Predator exposure schematic. Mice were placed in the presence of an awake rat restrained to one end of a chamber. Each exposure lasted 10 min. (D-K) Chemogenetic inhibition of l/vlPAG cck cells increased time spent in threat zone (D, unpaired t-test, *p=0.0199), increased number of approaches toward the rat (F, unpaired t-test, *p=0.0496), and reduced escape velocity from the rat (H, unpaired t-test, *p=0.0431). Threat distance trended toward significance with CCK inhibition (E, unpaired t-test, $^{\#}p = 0.069$). Approach velocity (G), stretch-attend postures (I), freezing (J), and distance travelled (K) were unaltered with inhibition (D-F, I-K: mCherry, n = 8; hM4Di, n = 12; G: mCherry, n = 5, hM4Di, n = 9; H: mCherry, n = 7, hM4Di, n = 11). Mean ± SEM.

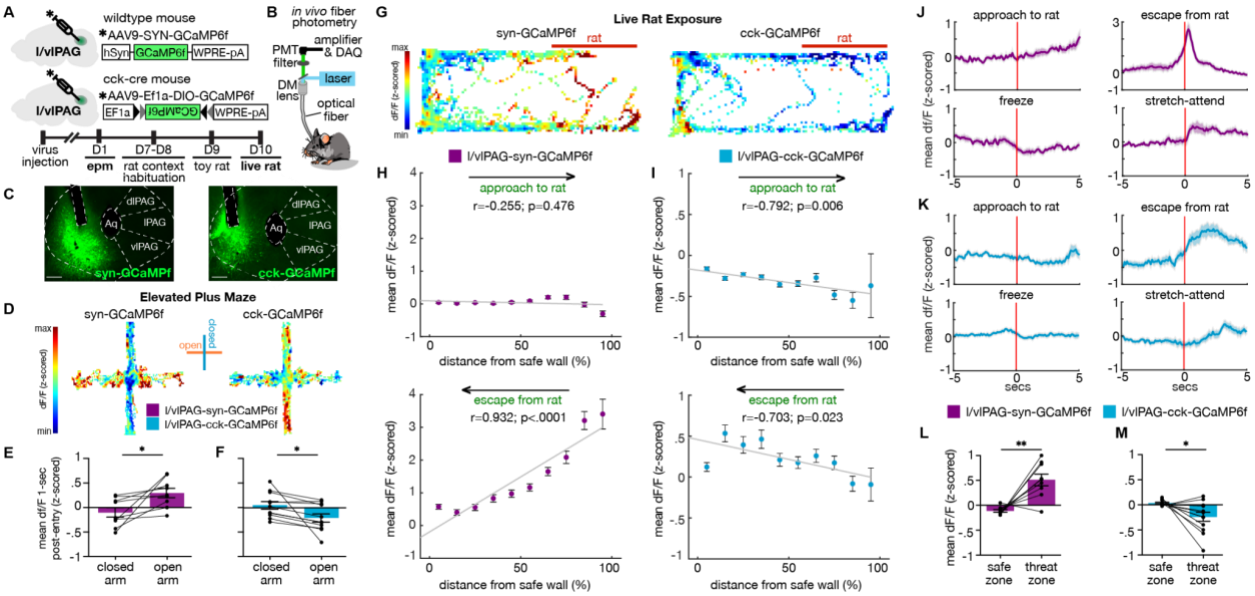

Figure 8. l/vlPAG-syn cells are more active near threat, while l/vlPAG-cck cells are more active far from threat. (A) Top, viral schematic for synapsin-specific and cck-specific GCaMP6 expression in l/vlPAG. Bottom, timeline for in vivo photometry recordings. (B) Fiber photometry recording set-up. (C) Histology of GCaMP6f expression in synapsin-specific (left) and cck-specific (right) cells in the l/vlPAG. Scale bar, 200µm. (D) Example heat maps showing z-scored dF/F in mice expressing synapsin-specific GCaMP6 (left) or cck-specific GCaMP6 (right) in l/vlPAG in an elevated plus maze assay. Vertical arms of heat maps represent closed arms. (E-F) Mean dF/F (z-scored) one-second after arm entry in syn-GCaMP6 (E) and cck-GCaMP6 mice (F). Mean dF/F 1-sec post-entry into the open arms is greater than into closed arms in syn-GCaMP6 mice (E, n = 9; paired t-test, *p=0.0213), whereas mean dF/F 1-sec post-entry into the open arms is lower than into the closed arms for cck-GCaMP6 mice (F, n = 11; paired t-test, *p=0.0283). (G) Example heat maps showing z-scored dF/F in syn-GCaMP6 (left) or cck-GCaMP6 (right) in Live Rat Exposure assay. Rat was confined to the right of the map, as indicated by the red bar. (H-I) Mean dF/F (z-scored) during approaches toward the rat (top) or escapes from the rat (bottom) within ten spatial bins of varying distance from the safe wall of syn-GCaMP6 (H, n = 9) or cck-GCaMP6 (I, n = 13) mice (syn-approach, n = 6744 samples; syn-escape, n = 2150 samples; cck-approach, n = 7170 samples; cck-escape, n = 2088 samples). (H) In syn-GCaMP6f mice, dF/F is positively correlated with distance from safe wall during escapes from the predator (Pearson's correlation coefficient r = 0.932, p < 0.0001). (I) In cck-GCaMP6f mice, dF/F is negatively correlated with distance from safe wall during both approaches and escapes (approach, r=-0.792, p=0.006; escape, r = -0.703, p = 0.023). (J-K) Mean dF/F (z-scored) 5-sec before and after approaches, escapes, freeze bouts, and stretch-attend postures in syn-GCaMP6 (L) and cck-GCaMP6 (M) populations (syn, n = 9; cck, n = 13 for freeze, n = 12 for other behaviors). (L-M) Mean dF/F (z-scored) in the safer zone (one-third of assay near safer wall) and threat zone (two-thirds of assay distal from safer wall) in syn-GCaMP6 (N) and cck-GCaMP6 (O) mice. Pan-neuronal l/vlPAG activity was increased in the threat zone compared to the safer zone (syn, n = 9; paired t-test, **p=0.0024), whereas cck-specific activity was decreased in the threat zone compared to the safer zone (cck, n = 12; paired t-test, *p=0.0223). Mean ± SEM.

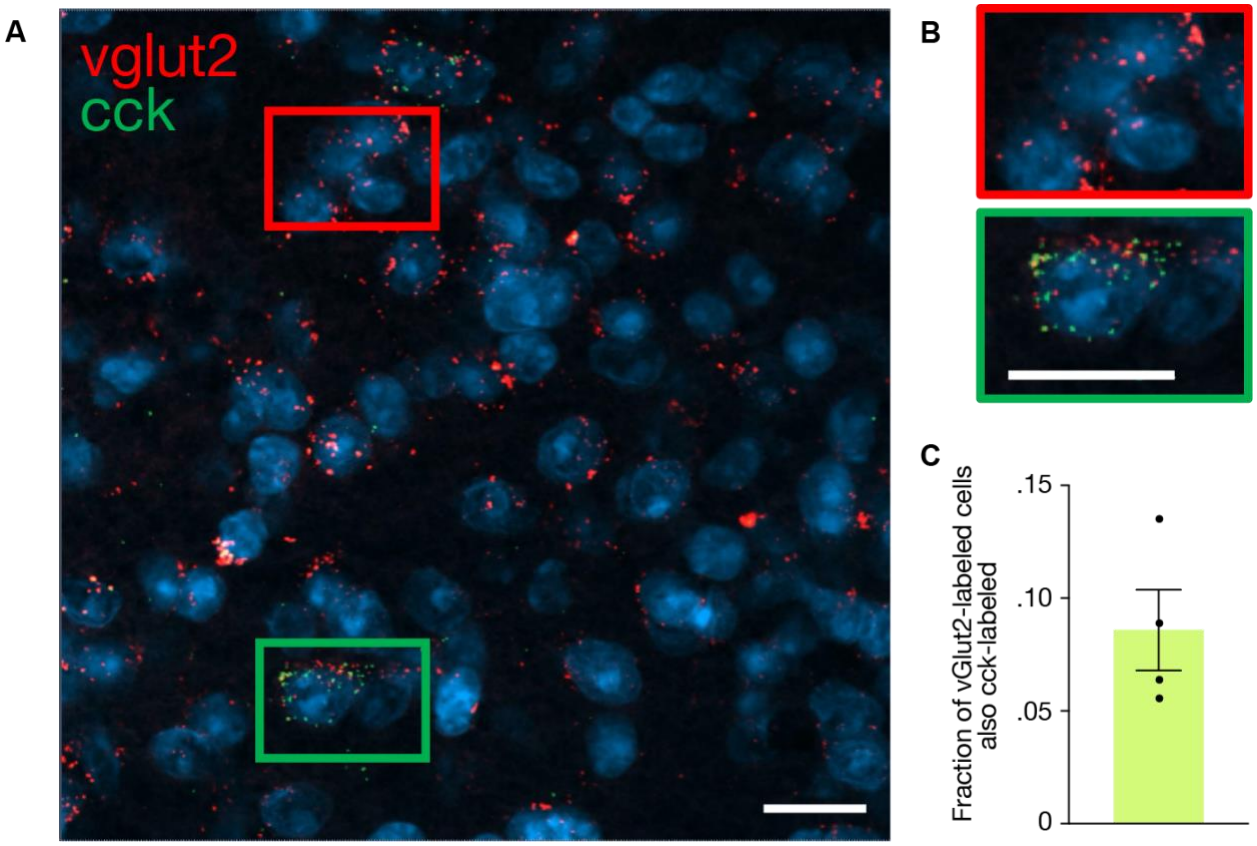

Figure 9. In situ hybridization of vglut2 and cck in the l/vlPAG shows double-labeling of vglut2 and cck. (A) In situ hybridization labelling of l/vlPAG neurons showing mRNAs for CCK (green) and VGLUT2 (red). Nuclei stained by DAPI are shown in blue. Example image (40x-objective) of vglut2-labeled cells (red rectangle) and double-labeled vglut2/cck-labeled (green rectangle) in l/vlPAG. Scale bar, 20um. (B) Zoomed in images of subregions in (A). Scale bar, 20um. (C) 8.58% of vglut2-labelled cells are also cck-labelled (15 of 183 total cells).

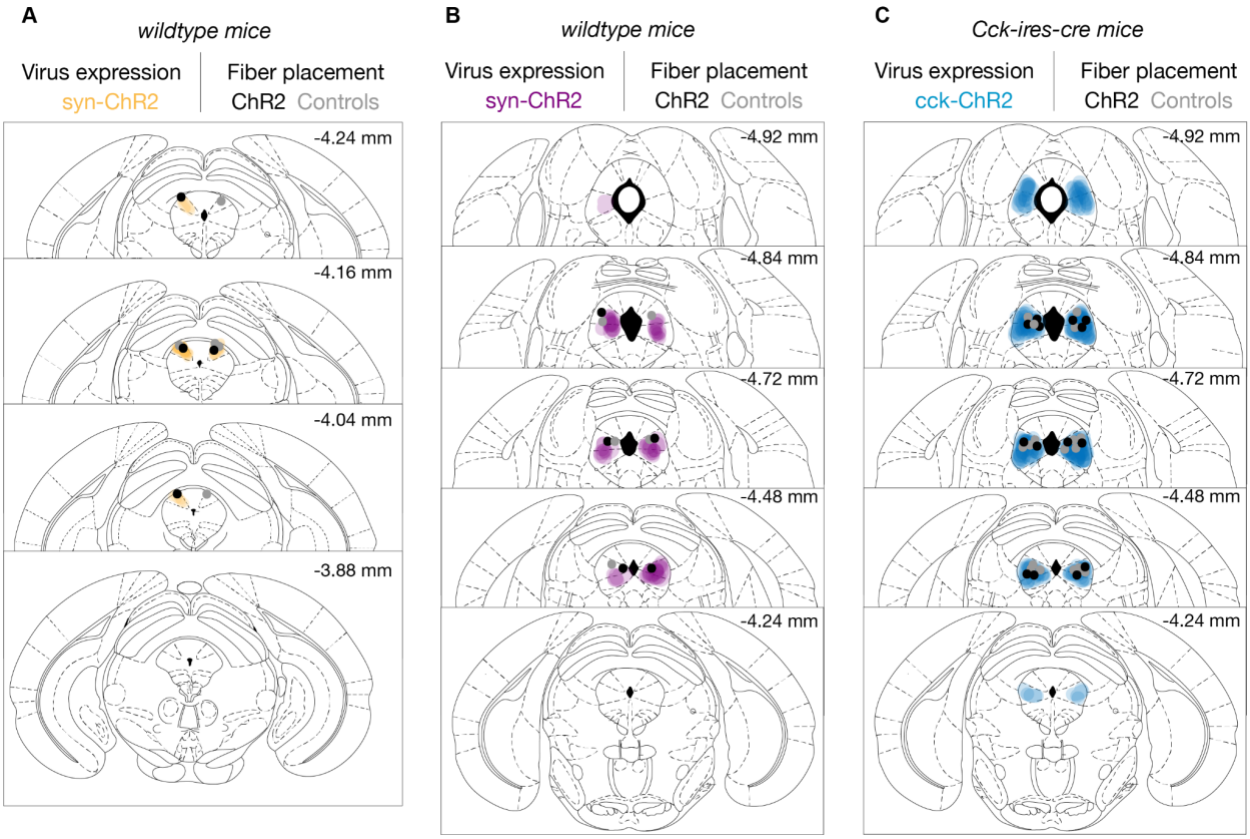

Figure 10. ChR2 expression and fiber placement in the PAG in coronal brain sections. ChR2 expression is depicted in shading and fiber placement is represented by dots for (A) dlPAG-syn mice, (B) l/vlPAG-syn mice, and (C) l/vlPAG-cck mice. Fibers targeting the l/vlPAG in (B) and (C) were placed at 15° angle. All fiber placements were unilateral and counterbalanced across left and right PAG. Center of fiber was determined at the widest point in histological slices.

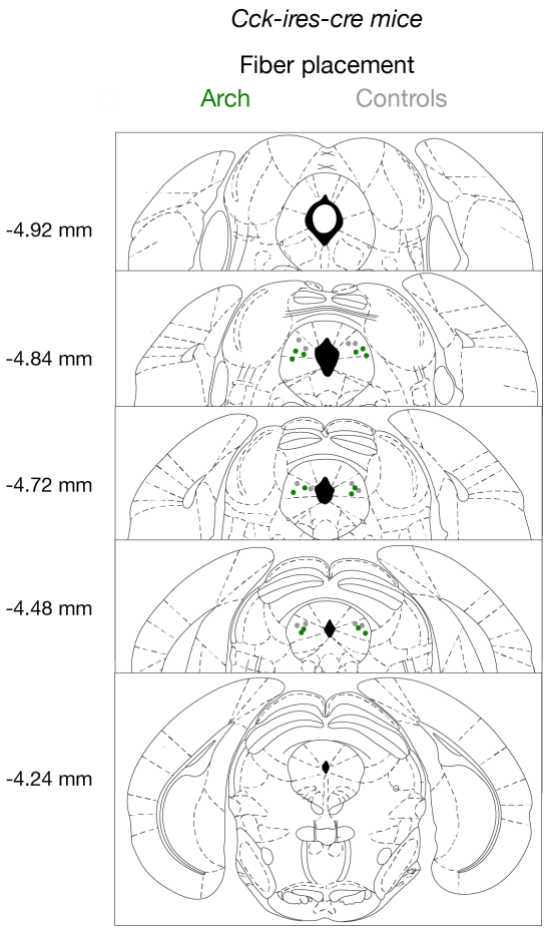

Figure 11. Bilateral fiber placement for optogenetic inhibition in coronal brain sections. Dots represent fiber placement in l/vlPAG-cck-Arch (green) or l/vlPAG-cck-GFP (grey) mice. All fiber placements were bilateral and placed at 15° angle. Center of fiber was determined at the widest point in histological slices.

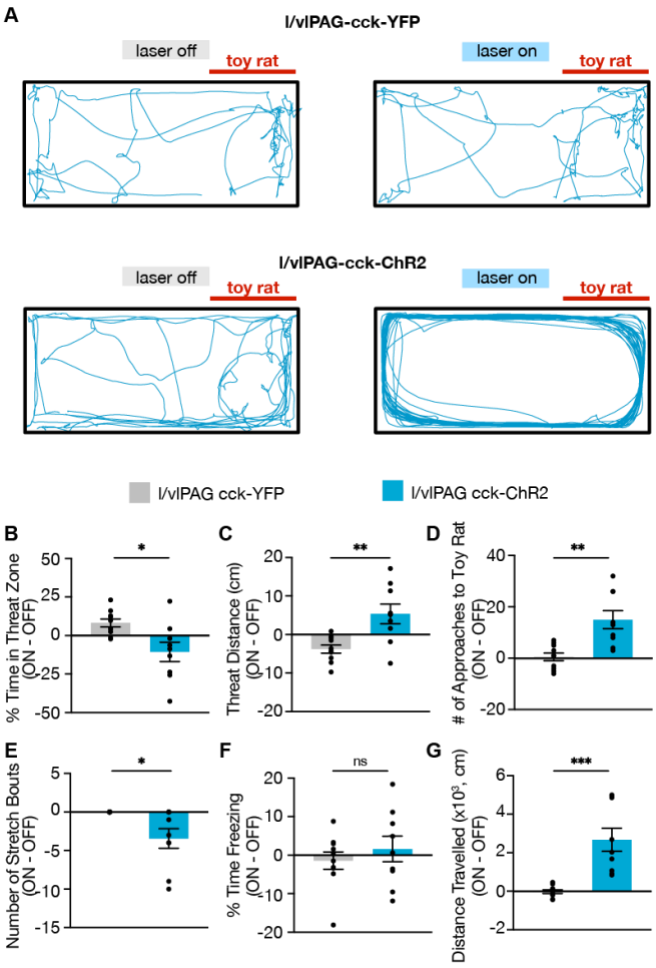

Figure 12. Optogenetic activation of l/vlPAG-cck neurons during toy rat exposure. (A). Example locomotion maps during laser-off (left) and laser-on (right) epochs of an l/vlPAG-cck-eYFP mouse (top) and an l/vlPAG-cck-ChR2-eYFP mouse (bottom). Stimulation induced robust traversal of all four corners of the enclosure (bottom-right). (B-G) Optogenetic stimulation of l/vlPAG-cck cells reduced time spent in threat zone (B, eYFP, n = 10, ChR2, n = 9; unpaired t-test, *p=0.0104), increased threat distance (C, eYFP, n = 10, ChR2, n = 9; unpaired t-test, **p=0.0032), increases number of approaches to the toy rat (D, eYFP, n = 10, ChR2, n = 9; unpaired t-test, **p=0.0011), reduced stretch bouts (E, eYFP, n = 10, ChR2, n = 9; unpaired t-test, *p=0.0107), and increased distance travelled (G, eYFP, n = 10, ChR2, n = 9; unpaired t-test, ***p=0.0002). Stimulation did not alter freezing (F). Mean ± SEM.

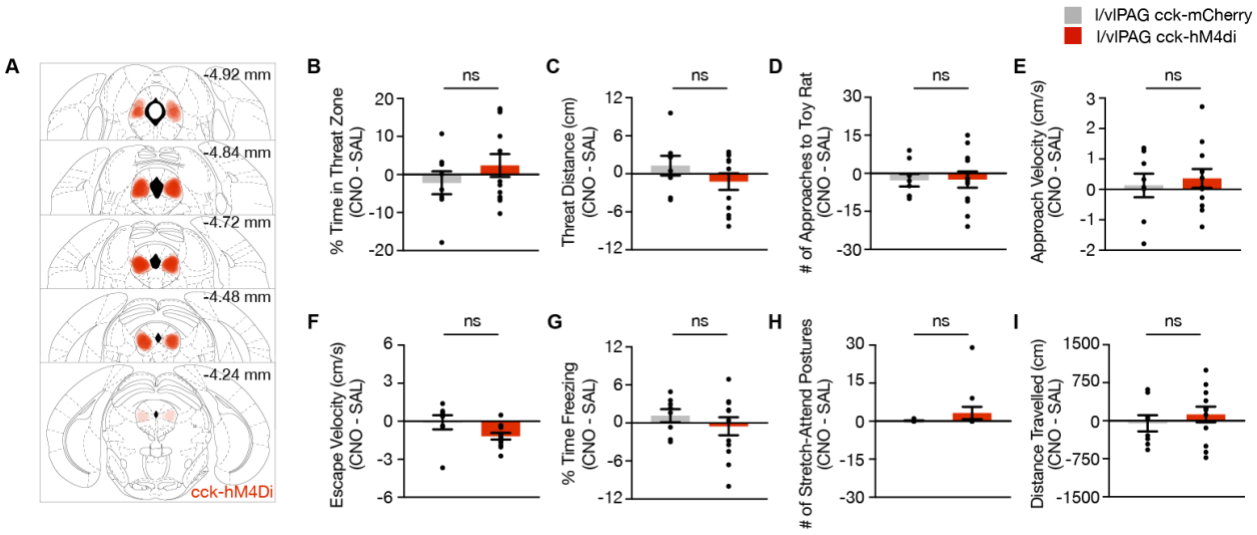

Figure 13. Chemogenetic of l/vlPAG-cck population using DREADDs during exposure to a toy rat. (A) Bilateral cre-dependent HM4Di expression in l/vlPAG of Cck-ires-cre mice. (B-I) Chemogenetic inhibition of l/vlPAG-cck cells during exposure to toy rat (mCherry, n = 8; hM4Di, n = 12; unpaired t-test). Mean ± SEM.

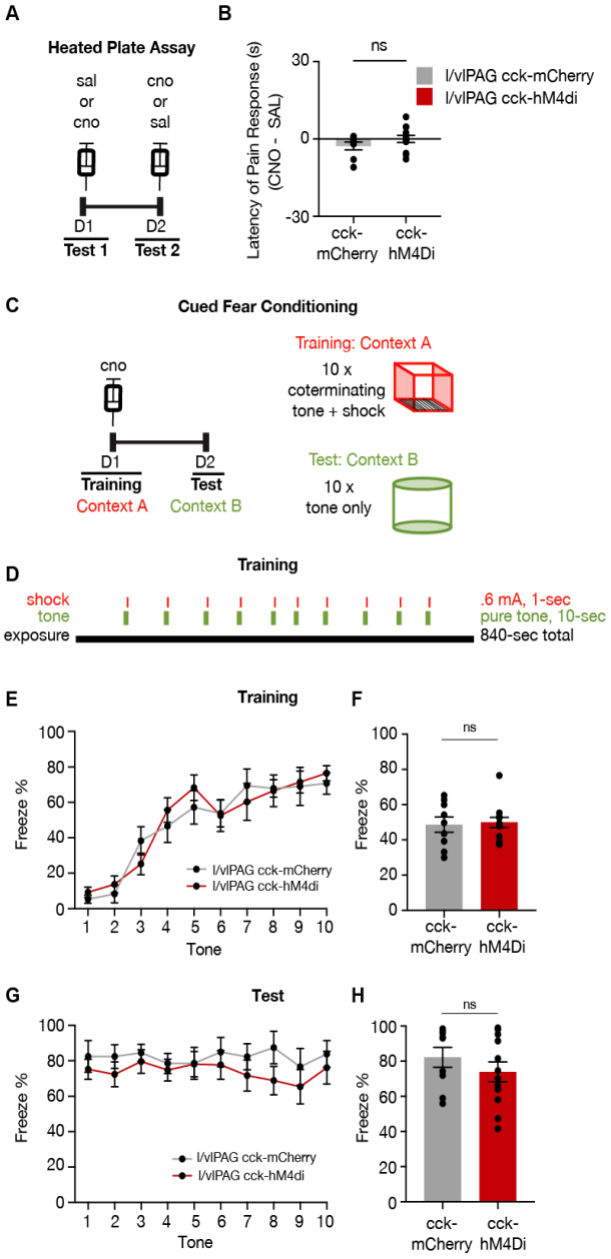

Figure 14. Inhibition of l/vlPAG-cck neurons does not alter pain response latency or acquisition of learned fear. (A) Timeline of heated plate assay with chemogenetic inhibition of l/vlPAG-cck cells. (B) Inhibition of l/vlPAG-cck cells does not alter latency of pain response (CNO minus saline; mCherry, n = 8; hM4Di, n = 12; unpaired t-test). Mean ± SEM. (C) Timeline of cued fear conditioning across two days (Training and Test) with l/vlPAG-cck chemogenetic inhibition during Training. Training occurred in Context A, which consisted of metal bar flooring, bare gray walls, warm-colored lighting and cleaned with 70% ethanol. Training included tone-shock pairings. Test occurred in Context B, which consisted of rounded white walls, gray smooth flooring, blue-colored lighting and cleaned with Strike-Bac. Both Contexts A and B were illuminated to 40-lux. Test included tone presentations only. (D) Schedule of tone and shock presentations during Training. Trial was 14-min in total, with ten pairs of co-terminating 10-sec tones and 1-sec shocks. The tone was a 70dB pure-tone and all shocks were 0.6 mA. (E) Mean freezing of cck-mCherry and cck-hM4Di mice during 10-sec tone presentations during Training (mCherry, n = 9; hM4Di, n = 12). (F) No difference in freezing during Training between groups (mCherry, n = 9; hM4Di, n = 12; unpaired t-test, p=0.799). (G) Same as E but during Test (mCherry, n = 9; hM4Di, n = 12). (H) Same as F but during Test (mCherry, n = 9; hM4Di, n = 12; unpaired t-test, p=0.328).

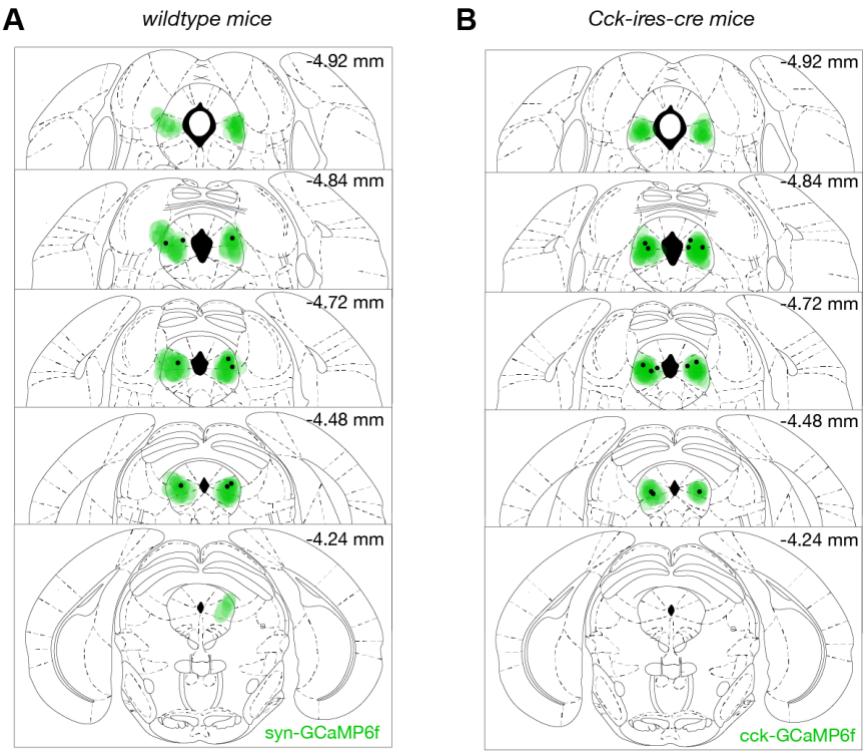

Figure 15. GCaMP6f expression and fiber placement in the l/vlPAG in coronal brain sections. GCaMP6f expression is depicted in shading and fiber placement is represented by dots for (A) l/vlPAG-syn mice and (B) l/vlPAG-cck mice. All fibers were placed at a 15° angle. All viral injections and fiber placements were unilateral and counterbalanced across left and right PAG. Center of fiber was determined at the widest point in histological slices.

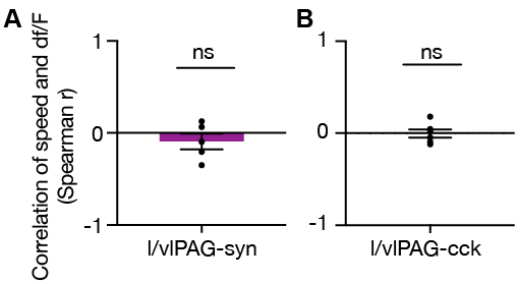

Figure 16. No correlation between speed and df/F. (A-B) Spearman correlation of speed and fiber photometry df/F of (A) l/vlPAG-synapsin or (B) l/vlPAG-cck population during exposure to toy rat (syn, n = 5; cck, n = 6; one-sample t-test). Mean ± SEM.

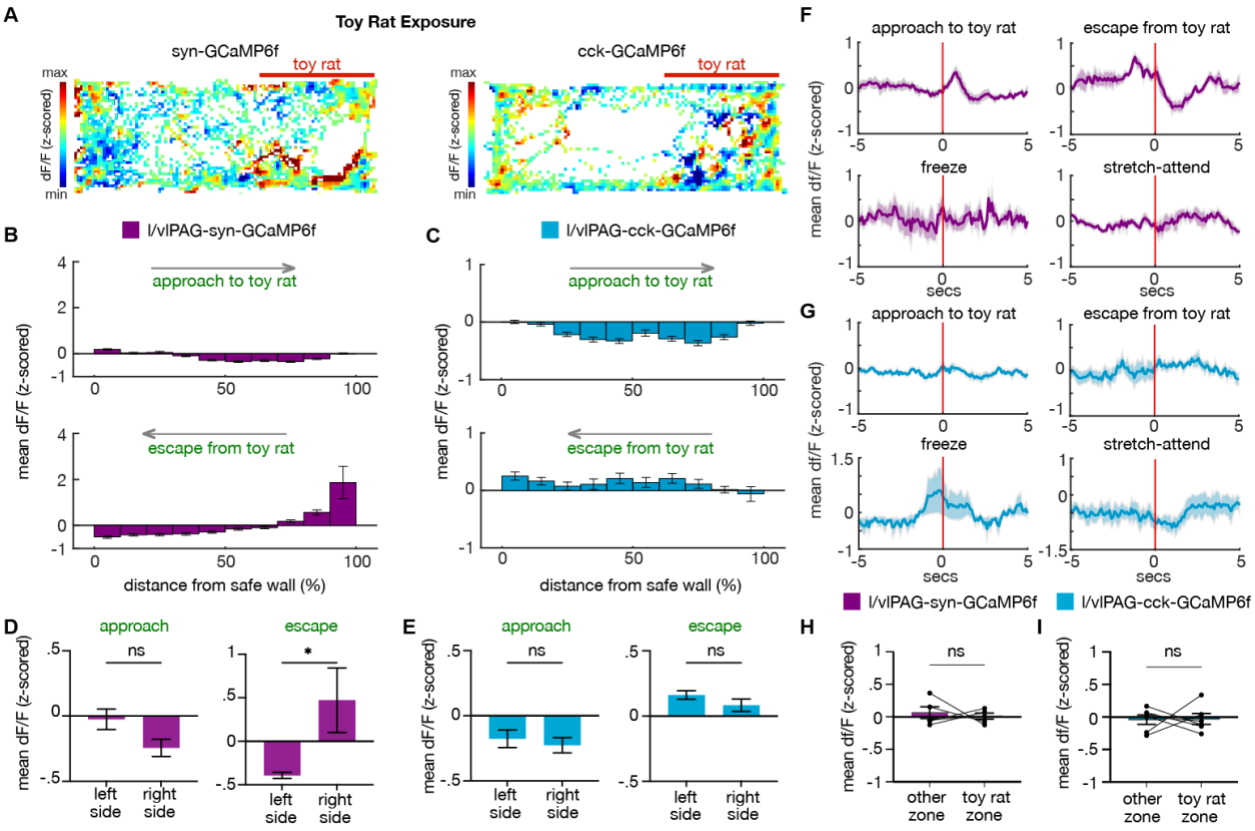

Figure 17. l/vlPAG-syn and cck activity during exposure to a control toy rat. (A) Example heat maps showing z-scored dF/F in syn-GCaMP6 (left) or cck-GCaMP6 (right) during exposure to a control toy rat. The toy rat was confined to the right of the map, as indicated by the red bar. (B-C) Mean dF/F (z-scored) during approaches toward the toy rat (top) or escapes from the toy rat (bottom) within ten spatial bins of varying distance from the safer wall of syn-GCaMP6 (B, n = 5) or cck-GCaMP6 (C, n = 6) mice (syn-approach, n = 7361 samples; syn-escape, n = 1884 samples; cck-approach, n = 3632 samples; cck-escape, n = 1128 samples). (D-E) Analysis of data shown in B-C, respectively. Comparisons of mean dF/F during approaches and escapes from toy rat from samples in the left or right side of the enclosure. The toy rat was located in the right side. Average of bins on right side is greater than average of bins on left side during escapes in syn-GCaMP6f mice (left side, n = 5 bins, right side, n = 5 bins; unpaired t-test, *p=0.0486). (F-G) Mean dF/F (z-scored) 5-sec before and after approaches, escapes, freeze bouts, and stretch-attend postures in syn-GCaMP6 (F, n = 5) and cck-GCaMP6 (G, n = 6) populations. (H-I) Mean dF/F (z-scored) in the third of the box near the wall and the toy rat zone (two-thirds of the environment near the toy rat) in syn-GCaMP6 (H) and cck-GCaMP6 (I) mice (syn, n = 5; cck, n = 6; paired t-test, ns = not significant). Mean ± SEM.

Acknowledgements

Results in this chapter were adapted from a manuscript published in *eLife*:

La-Vu, M., Sethi, E., Maesta-Pereira, S., Schuette, P., Tobias, B., Reis, F., Wang, W., Torossian, A., Bishop, A., Leonard, S., Lin, L., Cahill, C., Adhikari, A. Sparse genetically-defined neurons refine the canonical role of periaqueductal gray columnar organization. eLife. In press.

References

Aguiar DC, Guimarães FS. 2009. Blockade of NMDA receptors and nitric oxide synthesis in the dorsolateral periaqueductal gray attenuates behavioral and cellular responses of rats exposed to a live predator. J Neurosci Res 87:2418–2429.

Allen Institute for Brain Science (2021). Allen Mouse Brain Atlas. Available from mouse.brain-map.org.

Araki T, Yamano M, Murakami T, Wanaka A, Betz H, Tohyama M. 1988. Localization of glycine receptors in the rat central nervous system: an immunocytochemical analysis using monoclonal antibody. Neuroscience 25:613–624.

Assareh N, Sarrami M, Carrive P, McNally GP. 2016. The organization of defensive behavior elicited by optogenetic excitation of rat lateral or ventrolateral periaqueductal gray. Behav Neurosci 130:406–414.

Bandler R, Carrive P. 1988. Integrated defence reaction elicited by excitatory amino acid microinjection in the midbrain periaqueductal grey region of the unrestrained cat. Brain Res 439:95–106.

Bandler R, Depaulis A, Vergnes M. 1985. Identification of midbrain neurones mediating defensive behaviour in the rat by microinjections of excitatory amino acids. Behav Brain Res 15:107–119.

Bandler R, Shipley MT. 1994. Columnar organization in the midbrain periaqueductal gray: modules for emotional expression? Trends Neurosci 17:379–389.

Barbaresi P. 2005. GABA-immunoreactive neurons and terminals in the cat periaqueductal gray matter: a light and electron microscopic study. J Neurocytol 34:471–487.

Behbehani MM. 1995. Functional characteristics of the midbrain periaqueductal gray. Prog Neurobiol 46:575–605.

Bittencourt AS, Carobrez AP, Zamprogno LP, Tufik S, Schenberg LC. 2004. Organization of single components of defensive behaviors within distinct columns of periaqueductal gray matter of the rat: role of N-methyl-D-aspartic acid glutamate receptors. Neuroscience 125:71–89.

Bittencourt AS, Nakamura-Palacios EM, Mauad H, Tufik S, Schenberg LC. 2005. Organization of electrically and chemically evoked defensive behaviors within the deeper collicular layers as compared to the periaqueductal gray matter of the rat. Neuroscience 133:873–892.

Canteras NS, Goto M. 1999. Fos-like immunoreactivity in the periaqueductal gray of rats exposed to a natural predator. Neuroreport 10:413–418.

Carrive P. 1993. The periaqueductal gray and defensive behavior: functional representation and neuronal organization. Behav Brain Res 58:27–47.

de Andrade Rufino R, Mota-Ortiz SR, De Lima MAX, Baldo MVC, Canteras NS. 2019. The rostrodorsal periaqueductal gray influences both innate fear responses and acquisition of fear memory in animals exposed to a live predator. Brain Struct Funct 224:1537–1551.

Del-Ben CM, Graeff FG. 2009. Panic disorder: is the PAG involved? Neural Plast 2009:108135.
Deng H, Xiao X, Wang Z. 2016. Periaqueductal Gray Neuronal Activities Underlie Different Aspects of Defensive Behaviors. J Neurosci 36:7580–7588.

Depaulis A, Keay KA, Bandler R. 1992. Longitudinal neuronal organization of defensive reactions in the midbrain periaqueductal gray region of the rat. Exp Brain Res 90:307–318.

Evans DA, Stempel AV, Vale R, Ruehle S, Lefler Y, Branco T. 2018. A synaptic threshold mechanism for computing escape decisions. Nature 558:590–594.

Fadok JP, Krabbe S, Markovic M, Courtin J, Xu C, Massi L, Botta P, Bylund K, Müller C, Kovacevic A, Tovote P, Lüthi A. 2017. A competitive inhibitory circuit for selection of active and passive fear responses. Nature 542:96–100.

Fanselow MS. 1991. The Midbrain Periaqueductal Gray as a Coordinator of Action in Response to Fear and Anxiety In: Depaulis A, Bandler R, editors. The Midbrain Periaqueductal Gray Matter: Functional, Anatomical, and Neurochemical Organization. Boston, MA: Springer US. pp. 151–173.

Fanselow MS, Decola JP, De Oca BM, Landeira-Fernandez J. 1995. Ventral and dorsolateral regions of the midbrain periaqueductal gray (PAG) control different stages of defensive behavior: Dorsolateral PAG lesions enhance the defensive freezing produced by massed and immediate shock. Aggress Behav 21:63–77.

Felix-Ortiz AC, Beyeler A, Seo C, Leppla CA, Wildes CP, Tye KM. 2013. BLA to vHPC inputs modulate anxiety-related behaviors. Neuron 79:658–664.

Gao Z-R, Chen W-Z, Liu M-Z, Chen X-J, Wan L, Zhang X-Y, Yuan L, Lin J-K, Wang M, Zhou L, Xu X-H, Sun Y-G. 2019. Tac1-Expressing Neurons in the Periaqueductal Gray Facilitate the Itch-Scratching Cycle via Descending Regulation. Neuron 101:45–59.e9.

Gross CT, Canteras NS. 2012. The many paths to fear. Nat Rev Neurosci 13:651–658.

Guimarães FS, Carobrez AP, De Aguiar JC, Graeff FG. 1991. Anxiolytic effect in the elevated plus-maze of the NMDA receptor antagonist AP7 microinjected into the dorsal periaqueductal grey. Psychopharmacology 103:91–94.

Herkenham M, Lynn AB, Johnson MR, Melvin LS, de Costa BR, Rice KC. 1991. Characterization and localization of cannabinoid receptors in rat brain: a quantitative in vitro autoradiographic study. J Neurosci 11:563–583.

Herry C, Johansen JP. 2014. Encoding of fear learning and memory in distributed neuronal circuits. Nat Neurosci 17:1644–1654.

Jenck F, Moreau JL, Martin JR. 1995. Dorsal periaqueductal gray-induced aversion as a simulation of panic anxiety: elements of face and predictive validity. Psychiatry Res 57:181–191.

Johansen JP, Tarpley JW, LeDoux JE, Blair HT. 2010. Neural substrates for expectation-modulated fear learning in the amygdala and periaqueductal gray. Nat Neurosci 13:979–986.

Keay KA, Bandler R. 2015. Chapter 10 - Periaqueductal Gray In: Paxinos G, editor. The Rat Nervous System (Fourth Edition). San Diego: Academic Press. pp. 207–221.

Kepecs A, Fishell G. 2014. Interneuron cell types are fit to function. Nature 505:318–326.

Kim J, Pignatelli M, Xu S, Itohara S, Tonegawa S. 2016. Antagonistic negative and positive neurons of the basolateral amygdala. Nat Neurosci 19:1636–1646.

La-Vu M, Tobias BC, Schuette PJ, Adhikari A. 2020. To Approach or Avoid: An Introductory Overview of the Study of Anxiety Using Rodent Assays. Front Behav Neurosci 14:145.

Leman S, Dielenberg RA, Carrive P. 2003. Effect of dorsal periaqueductal gray lesion on cardiovascular and behavioural responses to contextual conditioned fear in rats. Behav Brain Res 143:169–176.

Liu H, Chandler S, Beitz AJ, Shipley MT, Behbehani MM. 1994. Characterization of the effect of cholecystokinin (CCK) on neurons in the periaqueductal gray of the rat: immunocytochemical and in vivo and in vitro electrophysiological studies. Brain Res 642:83–94.

Liu RP, Swenberg ML. 1988. Autoradiographic localization of substance P ligand binding sites and distribution of immunoreactive neurons in the periaqueductal gray of the rat. Brain Res 475:73–79.

Li Y, Zeng J, Zhang J, Yue C, Zhong W, Liu Z, Feng Q, Luo M. 2018. Hypothalamic Circuits for Predation and Evasion. Neuron 97:911–924.e5.

Lovett-Barron M, Andalman AS, Allen WE, Vesuna S, Kauvar I, Burns VM, Deisseroth K. 2017. Ancestral Circuits for the Coordinated Modulation of Brain State. Cell 171:1411–1423.e17.

Mascagni F, McDonald AJ. 2003. Immunohistochemical characterization of cholecystokinin containing neurons in the rat basolateral amygdala. Brain Res 976:171–184.

McNally GP, Johansen JP, Blair HT. 2011. Placing prediction into the fear circuit. Trends Neurosci 34:283–292.

Mendes-Gomes J, Motta SC, Passoni Bindi R, de Oliveira AR, Ullah F, Baldo MVC, Coimbra NC, Canteras NS, Blanchard DC. 2020. Defensive behaviors and brain regional activation changes in rats confronting a snake. Behav Brain Res 381:112469.

Mobbs D, Petrovic P, Marchant JL, Hassabis D, Weiskopf N, Seymour B, Dolan RJ, Frith CD. 2007. When fear is near: threat imminence elicits prefrontal-periaqueductal gray shifts in humans. Science 317:1079–1083.

Mobbs D, Yu R, Rowe JB, Eich H, FeldmanHall O, Dalgleish T. 2010. Neural activity associated with monitoring the oscillating threat value of a tarantula. Proc Natl Acad Sci U S A 107:20582–20586.

Molchanov ML, Guimarães FS. 2002. Anxiolytic-like effects of AP7 injected into the dorsolateral or ventrolateral columns of the periaqueductal gray of rats. Psychopharmacology 160:30–38.

Morgan MM, Clayton CC. 2005. Defensive behaviors evoked from the ventrolateral periaqueductal gray of the rat: comparison of opioid and GABA disinhibition. Behav Brain Res 164:61–66.

Motta SC, Carobrez AP, Canteras NS. 2017. The periaqueductal gray and primal emotional processing critical to influence complex defensive responses, fear learning and reward seeking. Neurosci Biobehav Rev 76:39–47.

Nath T, Mathis A, Chen AC, Patel A, Bethge M, Mathis MW. 2019. Using DeepLabCut for 3D markerless pose estimation across species and behaviors. Nat Protoc 14:2152–2176.

Netto CF, Guimarães FS. 2004. Anxiogenic effect of cholecystokinin in the dorsal periaqueductal gray. Neuropsychopharmacology 29:101–107.

Nguyen R, Venkatesan S, Binko M, Bang JY, Cajanding JD, Briggs C, Sargin D, Imayoshi I, Lambe EK, Kim JC. 2020. Cholecystokinin-Expressing Interneurons of the Medial Prefrontal Cortex Mediate Working Memory Retrieval. J Neurosci 40:2314–2331.

Ozawa T, Ycu EA, Kumar A, Yeh L-F, Ahmed T, Koivumaa J, Johansen JP. 2017. A feedback neural circuit for calibrating aversive memory strength. Nat Neurosci 20:90–97.

Perusini JN, Fanselow MS. 2015. Neurobehavioral perspectives on the distinction between fear and anxiety. Learn Mem 22:417–425.

Reis FMCV, Liu J, Schuette PJ, Lee JY, Maesta-Pereira S, Chakerian M, Wang W, Canteras NS, Kao JC, Adhikari A. 2021. Shared Dorsal Periaqueductal Gray Activation Patterns during Exposure to Innate and Conditioned Threats. J Neurosci 41:5399–5420.

Reis FM, Lee JY, Maesta-Pereira S, Schuette PJ, Chakerian M, Liu J, La-Vu MQ, Tobias BC, Ikebara JM, Kihara AH, Canteras NS, Kao JC, Adhikari A. 2021. Dorsal periaqueductal gray ensembles represent approach and avoidance states. Elife 10. doi:10.7554/eLife.64934

Samineni VK, Grajales-Reyes JG, Copits BA, O'Brien DE, Trigg SL, Gomez AM, Bruchas MR, Gereau RW 4th. 2017. Divergent Modulation of Nociception by Glutamatergic and GABAergic

Neuronal Subpopulations in the Periaqueductal Gray. eNeuro 4. doi:10.1523/ENEURO.0129-16.2017

Silva C, McNaughton N. 2019. Are periaqueductal gray and dorsal raphe the foundation of appetitive and aversive control? A comprehensive review. Prog Neurobiol 177:33–72.

Stujenske JM, Spellman T, Gordon JA. 2015. Modeling the Spatiotemporal Dynamics of Light and Heat Propagation for In Vivo Optogenetics. Cell Rep 12:525–534.

Tomaz C, Brandão M, Bagri A, Carrive P, Schmitt P. 1988. Flight behavior induced by microinjection of GABA antagonists into periventricular structures in detelencephalated rats. Pharmacol Biochem Behav 30:337–342.

Tovote P, Esposito MS, Botta P, Chaudun F, Fadok JP, Markovic M, Wolff SBE, Ramakrishnan C, Fenno L, Deisseroth K, Herry C, Arber S, Lüthi A. 2016. Midbrain circuits for defensive behaviour. Nature 534:206–212.

Tye KM, Prakash R, Kim S-Y, Fenno LE, Grosenick L, Zarabi H, Thompson KR, Gradinaru V, Ramakrishnan C, Deisseroth K. 2011. Amygdala circuitry mediating reversible and bidirectional control of anxiety. Nature 471:358–362.

Ullah F, dos Anjos-Garcia T, dos Santos IR, Biagioni AF, Coimbra NC. 2015. Relevance of dorsomedial hypothalamus, dorsomedial division of the ventromedial hypothalamus and the dorsal periaqueductal gray matter in the organization of freezing or oriented and non-oriented escape emotional behaviors. Behav Brain Res 293:143–152.

Valenstein ES. 1965. INDEPENDENCE OF APPROACH AND ESCAPE REACTIONS TO ELECTRICAL STIMULATION OF THE BRAIN. J Comp Physiol Psychol 60:20–30.

Walker P, Carrive P. 2003. Role of ventrolateral periaqueductal gray neurons in the behavioral and cardiovascular responses to contextual conditioned fear and poststress recovery. Neuroscience 116:897–912.

Walker RA, Wright KM, Jhou TC, McDannald MA. 2020. The ventrolateral periaqueductal grey updates fear via positive prediction error. Eur J Neurosci 51:866–880.

Wang W, Schuette PJ, La-Vu MQ, Torossian A, Tobias BC, Ceko M, Kragel PA, Reis FM, Ji S, Sehgal M, Maesta-Pereira S, Chakerian M, Silva AJ, Canteras NS, Wager T, Kao JC, Adhikari A. 2021a. Dorsal premammillary projection to periaqueductal gray controls escape vigor from innate and conditioned threats. Elife 10. doi:10.7554/eLife.69178

Wang W, Schuette PJ, Nagai J, Tobias BC, Cuccovia V Reis FM, Ji S, de Lima MAX, La-Vu MQ, Maesta-Pereira S, Chakerian M, Leonard SJ, Lin L, Severino AL, Cahill CM, Canteras NS, Khakh BS, Kao JC, Adhikari A. 2021. Coordination of escape and spatial navigation circuits orchestrates versatile flight from threats. Neuron 109:1848–1860.e8.

Watson TC, Cerminara NL, Lumb BM, Apps R. 2016. Neural Correlates of Fear in the Periaqueductal Gray. J Neurosci 36:12707–12719.

Whissell PD, Cajanding JD, Fogel N, Kim JC. 2015. Comparative density of CCK- and PV-GABA cells within the cortex and hippocampus. Front Neuroanat 9:124.

Yang Y-M, Chung J-M, Rhim H. 2006. Cellular action of cholecystokinin-8S-mediated excitatory effects in the rat periaqueductal gray. Life Sci 79:1702–1711.

Yin J-B, Wu H-H, Dong Y-L, Zhang T, Wang J, Zhang Y, Wei Y-Y, Lu Y-C, Wu S-X, Wang W, Li Y-Q. 2014. Neurochemical properties of BDNF-containing neurons projecting to rostral ventromedial medulla in the ventrolateral periaqueductal gray. Front Neural Circuits 8:137.

Yu H, Xiang X, Chen Z, Wang X, Dai J, Wang X, Huang P, Zhao Z-D, Shen WL, Li H. 2021. Periaqueductal gray neurons encode the sequential motor program in hunting behavior of mice. Nat Commun 12:6523.

Zanoveli JM, Netto CF, Guimarães FS, Zangrossi H Jr. 2004. Systemic and intra-dorsal periaqueductal gray injections of cholecystokinin sulfated octapeptide (CCK-8s) induce a panic-like response in rats submitted to the elevated T-maze. Peptides 25:1935–1941.

Zhang SP, Bandler R, Carrive P. 1990. Flight and immobility evoked by excitatory amino acid microinjection within distinct parts of the subtentorial midbrain periaqueductal gray of the cat. Brain Res 520:73–82.